

8

Group 10 and 11 Transition Metal–Dinitrogen Complexes

Ricardo B. Ferreira and Leslie J. Murray

University of Florida, Department of Chemistry, 214 Leigh Hall, Gainesville, FL 32611-7200, USA

Group 10 and 11 transition metals are uniquely placed in the d-block elements as their electronegativities position these metals at the border of classic ligand field theory and the more covalent interactions typical of the p-block elements. The greater electronegativity as compared to that of the earlier transition metals is expected to afford weaker interactions with dinitrogen, and the isolation of such adducts is challenging if possible. The number of reported metal–dinitrogen complexes in these groups is expected to be scarce as the electronegativity correlates with decreased π -backdonation to a N_2 ligand. Such metal–ligand π -interactions are considered essential for generating isolable metal–dinitrogen species as well as affording significant activation of the $N\equiv N$ multiple bond. Despite these challenges, such compounds have been synthesized by the careful selection of ancillary ligands on the metal center, with aspects such as ligand electronic effects, steric constraints, and metal oxidation “states” proving critical. Details on the extent of activation of the dinitrogen fragment as a function of ligand type will be highlighted, with focus on their structure and reactivity relationships. In addition, the downstream reactivity of the dinitrogen adducts will be discussed insofar as the reactivity reports on the properties of the metal– N_2 adduct.

8.1 Introduction

Dinitrogen metal compounds were first reported by Allen and coworkers in the late 1960s, and since then, a vast library of compounds of this type has been synthesized and characterized. The interaction of this diatomic with metal centers usually occurs in an end-on coordination mode instead of a side-on arrangement (Figure 8.1). The end-on coordination allows for a more efficient σ -donation from the $3\sigma_g$ orbital in N_2 , which has pronounced $2p_z$ character, to the metal d-orbitals of appropriate symmetry (e.g. a d_{z^2} -orbital). Additionally, d-orbitals of the metal with π -type symmetry can engage in π -backdonation to the $1\pi_g$ orbitals in the N_2 fragment, which is antibonding in character. This π -backbonding expectedly leads to a weakening of the N–N bond, typically

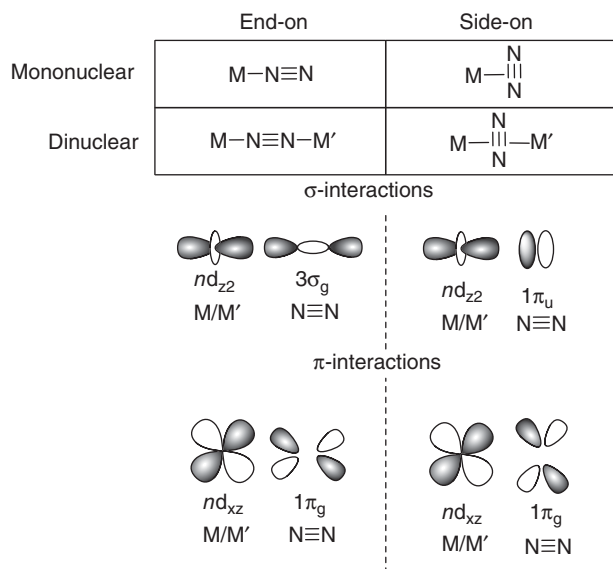


Figure 8.1 Schematic representation of the possible geometries found in metal–dinitrogen complexes (top) and examples of orbitals involved in the formation of σ - and π -interactions in end-on and side-on complexes (bottom).

manifested in bond elongation in structural data (e.g. X-ray or EXAFS) and a decrease in the N–N stretching frequency from free N_2 [1]. In contrast, the side-on interaction is observed exclusively in multimetallic systems; here, the $1\pi_u$ orbital of N_2 acts as the σ -bonding orbital with a π -backbonding interaction similar to that for an end-on coordination. Independent of the coordination mode, the π -backbonding interaction has been generally considered as critical for dinitrogen coordination to metal center(s).

Compared to the plethora of dinitrogen adducts for transition metals in groups 3–9, metal–dinitrogen compounds containing group 10 and 11 metals are relatively rare in the literature. These findings can be rationalized by substantially weaker π -backbonding interactions as a consequence of these metals having the greatest electronegativities of the d-block elements.

With this simplified model in mind, the typical routes employed to access dinitrogen complexes of these metals primarily rely on accessing coordinatively unsaturated metal centers followed by exposure to dinitrogen and strict avoidance of potential adventitious ligands (e.g. solvent). Specifically, ligand steric effects for discrete molecular species or solvent-free conditions for extended solids provide the necessary selective constraints for N_2 coordination over other possible ligands. For the group 10 metals, coordinative unsaturation is also coupled to low metal oxidation states (e.g. nickel(0) or (I)), which favor π -backbonding to and reduction of coordinated dinitrogen.

In the next sections, the synthesis and reactivity of group 10 and 11 metal–dinitrogen complexes will be discussed with focus on the type of interactions formed with dinitrogen with some consideration of the reactivity of these metal–dinitrogen complexes upon exposure to other substrates.

8.2 Group 10 Transition Metal–Dinitrogen Complexes

Group 10 transition metals (nickel, palladium, and platinum) are involved in the activation of several small molecules and are commonly employed in numerous organometallic catalytic processes. For example, these metals have been used extensively as catalysts for catalytic hydrogenations, C–H activation, and carbon–carbon cross-couplings [2, 3]. However, as it will become apparent in the next few sections, the interaction and activation of N₂ remains underexplored, likely for the electronic reasons outlined above.

Several examples in the literature show that, by selecting appropriate ligand systems, nickel can bind and activate N₂ and produce complexes that expand upon our understanding of the bonding between this diatomic and metal centers. Historically, nickel–dinitrogen chemistry was first studied in heterogeneous systems, and particularly Ni metal surfaces, which ultimately laid the foundation for the exploration of N₂ activation on Ni centers in molecular species in the 1970s. For this reason, the adsorption of dinitrogen on nickel surfaces will be covered in the next section followed by the discussion of discrete molecular systems.

8.2.1 Nickel

The interactions of nickel with small molecules have been explored in heterogeneous catalytic systems as part of detailed investigations of dihydrogen, olefin, and alkyne activation. Following this trend, the first study involving the association of nickel and N₂ occurred in the solid state using adsorption isotherms beginning in the 1940s with the most recent reports in the late 1980s [4, 5]. This initial foray into nickel–dinitrogen chemistry will be discussed in Section 8.2.1.1.

Molecular systems present unique advantages over the surface and material approaches outlined previously. In particular, well-developed spectroscopic and characterization methods can be readily applied to molecular species, such as single-crystal X-ray diffraction, infrared spectroscopy, and mass spectrometry. As expected then, the synthesis and characterization of molecular nickel–dinitrogen species could provide the atomistic understanding of the extent of metal π -backbonding to the bound dinitrogen, the strength of the metal–dinitrogen bond, and the parameters (e.g. ligand field) that modulate N₂ activation.

One of the most used ways to obtain such species is matrix-assisted isolation, which consists of the laser ablation of highly reactive metal compounds and the careful exposure to a substrate of interest – specifically, dinitrogen for this discussion – at cryogenic temperatures. This method of sample preparation is coupled to a selected characterization technique, such as infrared or Raman spectroscopy and mass spectrometry. Nickel–dinitrogen species obtained in the gas phase or in matrices and their associated spectroscopic characterization from these experiments will be discussed in Section 8.2.1.2. More recently, discrete nickel coordination compounds employing simple phosphine donors, meridional ligating or pincer ligands, triphosphine and tetrapodal ligands, and β -diketiminates have been reported to bind dinitrogen, providing a unique vantage to understand the

details of the Ni–N₂ bonding interaction. These systems will be discussed in Section 8.2.1.3.

8.2.1.1 Interaction of Dinitrogen with Nickel Surfaces

The adsorption studies of N₂ on nickel surfaces concluded that the interaction is best described as a weak chemisorption at low temperatures [6–16]. Many of these studies have shown that N₂ binds mostly to atop sites in an end-on coordination to the nickel atoms on the (110) plane; μ -1,2- or μ - η^2 : η^2 modes for N₂ bound to surface nickel atoms have been invoked in a more recent study.

Going from extended solids to small metal clusters, these studies were expanded to small neutral and cationic nickel clusters (Ni_{*x*}^{0/+}, *x* = 3–71) in the gas phase to provide a more precise picture of N₂ activation by metal surfaces as a function of crystal facet and as the means to elucidating the structure of such clusters [17–23]. Compared to the bulk nickel surfaces, the binding energy of N₂ to these clusters is two times higher (around –80 kJ mol^{–1} for these clusters), and there is a trend of enhancement of the N₂ interaction to the lower end of cluster size [20]. Even though all the mentioned studies take advantage of nickel in solid-state materials, they evidence that the stability and ease of formation of nickel–dinitrogen compounds can be tuned by their oxidation state and the local coordination environment. In the next section, complexes containing nickel centers will be evaluated in terms of binding affinity to N₂ and their extent of activation.

8.2.1.2 Matrix-Assisted Isolation of Binary or Ternary Compounds

Studies involving the interaction of N₂ with discrete laser-ablated nickel species date from 1970s [24–30]. The first species demonstrating nickel(0)–dinitrogen interactions could be observed by infrared spectroscopy. These species were generated from nickel metal targets and condensation of the ablated nickel atoms in the mixtures of N₂ and Ar at cryogenic temperatures. This method leverages that free N₂ is IR silent, whereas N₂ coordinated in an end-on manner leads to a dipole in the N₂ fragment, and consequently, an infrared-active N–N stretching mode is now observable. From those experiments, Turner and collaborators identified a Ni(N₂) species for which an IR-active vibration as the N–N stretching mode was recorded at 2089 cm^{–1}. This value is consistent with the end-on coordination of dinitrogen to nickel(0) from isotopic labeling experiments [25, 26]. In addition, species with a larger number of N₂ coordinated molecules were also identified with the formula Ni(N₂)_{*n*} (*n* = 2–4) and the vibrational data consistent with diminished π -backbonding to any single N₂ as expected [31–33]. For the tetrakis(dinitrogen) complex, vibrational data support tetrahedral arrangement of N₂ molecules around the nickel(0) site, which is reminiscent from the structural studies from the isoelectronic Ni(CO)₄ [27, 33].

In addition to laser ablation, binary species containing nickel and dinitrogen were also able to be generated using ion bombardment. Barber and Vickerman were evaluating the interaction of N₂O with nickel metal using secondary ion mass spectrometry [28]. Upon argon ion bombardment of a nickel foil in the presence of N₂O, these authors identified ions consistent with [Ni₂N₂]⁺, [Ni₂N]⁺, and [Ni₂O]⁺. Interestingly, they did not observe the presence of the

mononickel ion, $[\text{NiN}_2]^+$, the neutral analog of which was widely reported in laser ablation studies [31]. The authors concluded that the absence of the signal for the mononickel species results from the particular adsorption process of the nitrous oxide onto the metal surface, which preferentially adsorbs between two nickel atoms and perpendicular to the surface, thereby favoring the formation of dinickel ions. The formation of polymetallic species in these experiments can be viewed as a harbinger of the coordination chemistry that followed as polymetallic–dinitrogen compounds are very common.

The laser ablation method also allowed access to heteroleptic nickel(0) species of the type $\text{Ni}(\text{CO})_{4-m}(\text{N}_2)_m$, with $m = 1-3$. Such species were first observed by Rest who explored the photolysis of $\text{Ni}(\text{CO})_4$ in a matrix of N_2 at 20 K in 1972. Under these conditions, the author identified $\text{Ni}(\text{CO})_3(\text{N}_2)$ and assigned the absorption at 2266 cm^{-1} to the N–N stretching mode of a terminal $\eta^1\text{-N}_2$. This absorption has a high relative intensity, and the pattern of absorption relative to the CO stretching modes bears strong resemblance to that of a previously reported tricarbonyl(η^1 -nitrosyl)cobalt(0) compound, $(\text{Co}(\text{NO})(\text{CO})_3)$ [34]. Later, Ozin and coworkers also reported such species in laser ablation experiments on nickel metal followed by exposure to a mixture of CO and N_2 in frozen Ar or Kr matrices at temperatures ranging from 4 to 114 K. Their results corroborated and confirmed the end-on coordination mode in these heteroleptic species [34–36]. Following on these studies, Turner et al. explored the ligand competition using $\text{Ni}(\text{CO})_3(\text{N}_2)$ by observing the thermal decay of this species in the presence of CO to produce $\text{Ni}(\text{CO})_4$. These competition experiments allowed for the first estimates of the Ni– N_2 bond dissociation energy as c. 40 kJ mol^{-1} . The low value agrees with the observed minimal activation of the N_2 fragment in these molecules from vibrational data and is consistent with the anticipated poor backbonding afforded by the group 10 metals [36]. Another important factor is the presence of three strongly π -acidic carbonyl ligands bound to nickel, which decrease the electron density on the metal center further minimizing electron donation from the Ni center to the N_2 fragment.

Other than the matrix-assisted nickel(0)–dinitrogen compounds observed in the 1970s, Chen et al. reported the formation of the first nickel(I)–dinitrogen species obtained for this method in the 2000s. They relied on the laser-ablation of copper and nickel halides, followed by the reaction with dinitrogen, and isolation in a solid argon matrix, forming linear complexes of the type $\text{XM}(\text{N}_2)$ (where $X = \text{Cl, Br}$, and $M = \text{Cu, Ni}$). The products were characterized by infrared spectroscopy, and isotopic labeling confirmed the linear geometry of the molecules with N_2 in an end-on coordination mode bonded to the metal ion [37]. For the $\text{ClNi}(\text{N}_2)$ species, the N–N stretching mode was observed at 2246.1 cm^{-1} , indicating less activation of the N_2 fragment as compared to the matrix-isolated nickel(0) species (e.g. $\text{Ni}(\text{N}_2)$) previously discussed. These observations agree with the expected weaker π -backdonation for a less electron-rich metal center and, therefore, lower activation of the N_2 ligand. On the other hand, it is important to highlight that $\text{ClNi}(\text{N}_2)$ shows a higher degree of N_2 activation when compared to the nickel(0) compound $\text{Ni}(\text{CO})_3(\text{N}_2)$, evidencing that the coordination of strong π -acceptor ligands can have a more significant effect on the degree of N_2 activation than the formal oxidation state of the metal center.

Related to these nickel(I) halide species, Bridgeman et al. reported in 2000 the formation of nickel(II)–dinitrogen species by the laser ablation of NiCl_2 and NiBr_2 in a N_2 matrix. Under the conditions reported, the authors observed unstable pseudotetrahedral species of the type $\text{NiX}_2(\text{N}_2)_2$, with $X = \text{Cl}$ and Br . Interestingly, they observed absorptions in the infrared region in the range $2260\text{--}2280\text{ cm}^{-1}$, which were assigned to N–N stretching modes. The relatively unactivated N_2 ligands in these species are consistent with the higher oxidation state of the nickel centers in these compounds (viz +2 oxidation state). Consistently, the values of $\nu_{\text{N-N}}$ for the chloride derivative are slightly lower than those for the bromide derivative, implying a more electron-rich nickel center as better π -donation from the halide to nickel for chloride is expected with $3\text{p}\text{--}3\text{d}$ overlap ($\text{Cl}\text{--Ni}$) as being greater than $4\text{p}\text{--}3\text{d}$ overlap ($\text{Br}\text{--Ni}$) [38].

8.2.1.3 Coordination Compounds

In contrast to the more common η^1 -dinitrogen donors in the matrix-isolated species, the first examples of nickel–dinitrogen coordination complexes – reported in the 1970s – evidenced a $\mu\text{--}\eta^2\text{:}\eta^2$ coordination mode for dinitrogen with alkali cations coordinated in an η^1 or end-on manner to the dinitrogen ligand [39–41]. The alkali cations are key components of these compounds as they result in a push–pull effect to weaken the N–N bond; the alkali cations polarize the dinitrogen ligand, thereby enhancing π -backdonation from the nickel centers into the N_2 fragment. Indeed, the N–N bond distances found in these nickel–dinitrogen complexes ($1.35\text{--}1.36\text{ \AA}$) are the longest known for nickel complexes and foreshadow current interest in coupling redox innocent cations with small-molecule activation at transition metal centers [42].

At a similar time period, exploration of the chemistry of trialkylphosphine-supported nickel(0) complexes by Tolman et al. led to the discovery of a family of nickel–dinitrogen species. Although many of these compounds were not structurally characterized, ^{31}P -NMR and IR methods provided strong and substantive support for dinitrogen ligation. Tolman et al. noted that although ligand dissociation is slow and recalcitrant for tetrakis(trimethyl)phosphine nickel(0), the analogous triethylphosphine complex readily dissociates one phosphine in organic solvents under argon to produce the dark violet $\text{Ni}(\text{PEt}_3)_3$. This coordinatively unsaturated species could be readily isolated under reduced pressures (Figure 8.2) [43]. However, the dark violet color of the three-coordinate complex fades in the presence of N_2 , affording a new IR absorption feature at $\sim 2065\text{ cm}^{-1}$. The energy of this absorption is consistent with the matrix-isolated end-on dinitrogen complexes, and isotopic labeling confirmed the identity of the product as $(\text{Et}_3\text{P})_3\text{Ni}(\text{N}_2)$ [44].

The seminal report of a structurally characterized complex with $\text{Ni}\text{--N}_2$ interactions was by Jonas and coworker in 1968. Reaction of bis(acetylacetonato) nickel(II) with trimethylaluminum in the presence of a tricyclohexylphosphine under a dinitrogen atmosphere produced a dinitrogen nickel(0) complex, $\text{Ni}(\text{PCy}_3)_2(\text{N}_2)$ ($\text{Cy} = \text{cyclohexyl}$). This formula was confirmed by cryogenic molecular-weight determination, and this reaction proceeds with the appearance of a new infrared absorption at 2028 cm^{-1} , attributed to the N–N stretching of the coordinated N_2 molecule [45, 46]. In addition, an equilibrium between

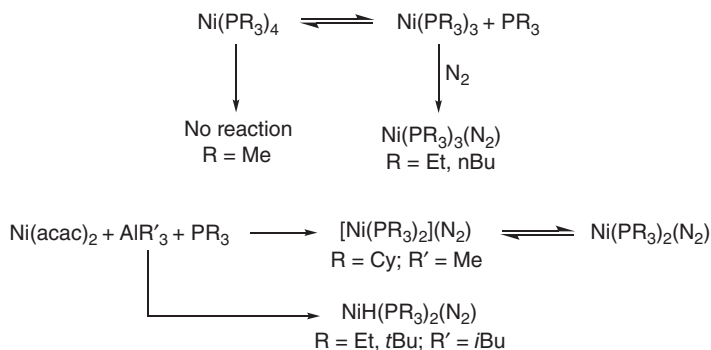


Figure 8.2 Synthesis of dinitrogen-bound nickel(0/I) complexes with trialkylphosphines.

this species and a dinuclear complex containing a Ni–(N₂)–Ni interaction was observed. The solid state structures of the monomeric and dimeric products were also determined, the latter of which is reminiscent of the work of Barber et al. The same dinickel species could also be prepared by the reduction of Ni(PCy₃)₂Br₂ with excess Na under N₂. No absorption in the infrared was observed for [Ni(PCy₃)₂]₂(N₂), which is in agreement with the pseudoinversion symmetry of the Ni₂(N₂) fragment within the complex [46, 47].

The coordinated N₂ molecule in [Ni(PCy₃)₂]₂(N₂) can be readily displaced by olefins, such as ethylene or 1,5,9-cyclododecatriene. In those experiments, ligand substitution occurs with the release of 0.5 equiv of N₂ per equivalent of nickel(0), consistent with a Ni:N₂ ratio of 2 : 1 [46]. Thiophenols (ArSH) also react with [Ni(PCy₃)₂]₂(N₂) resulting in the release of N₂ and the formation of *trans*-NiH(ArS)(PCy₃)₂ by formal oxidative addition across the S–H bond [48].

These examples suggest a weak interaction between N₂ and Ni(0), with ligands that undergo oxidative addition or are better π-acceptors resulting in the substitution of N₂. Surprisingly, however, Aresta et al. observed that dissolution of a carbon dioxide complex, Ni(PCy₃)₂(CO₂), under dinitrogen gave rise to an equilibrium between the CO₂- and N₂-bridged dimers. Because of the formation of some amount of this nickel–dinitrogen adduct, yields for the subsequent CO₂ reduction to CO when exposed to Brønsted acids were lower than in the absence of N₂. These results highlighted that the nickel(0)–dinitrogen interactions, albeit weak, cannot be neglected as adduct formation can influence further reactivity [49].

Phosphines were considered ideal ligands in the early nickel dinitrogen chemistry as their strong σ donor ability affords a more electron-rich metal center, which can consequently π-backbond more effectively to a dinitrogen ligand. More recently, Beck et al. proposed a different route for obtaining nickel(0)–dinitrogen complexes from nickel(I) precursors [50]. Starting with the comproportionation of bis(triisopropylphosphine)nickel(II) dichloride and [η²-ethylene-bis(triisopropylphosphine)nickel(0)], they reported the synthesis of a nickel(I) chloride species, Ni(ⁱPr₃P)₂Cl. Upon reduction using magnesium under N₂, this nickel(I) compound produced a dimer [Ni(ⁱPr₃P)₂]₂(N₂) of structure similar to the one obtained with PCy₃. Interestingly, this compound

showed a band in the Raman spectrum lying around 1908 cm^{-1} assigned to the N–N stretching vibrational mode, which is a very low value compared to other nickel compounds. In fact, the N–N bond distance in the crystal structure of $[\text{Ni}(\text{P}^i\text{Pr}_3)_2]_2(\text{N}_2)$ is $1.158(5)\text{ \AA}$, which agrees with substantial activation of the dinitrogen fragment. Unlike the corresponding compound obtained with PCy_3 reported by Jonas and coworkers [45, 46], the authors did not observe the formation of the mononuclear species in solution. The proposed rationale for the enhanced activation of the N_2 fragment for $[\text{Ni}(\text{P}^i\text{Pr}_3)_2]_2(\text{N}_2)$ vis-à-vis $[\text{Ni}(\text{PCy}_3)_2]_2(\text{N}_2)$ is the structural differences afforded by the phosphine substituents. Despite the similar Tolman cone angles for PCy_3 and P^iPr_3 (viz 170° and 160° , respectively), the dihedral angles formed by the PNiP planes in these complexes are approximately 105° and 81° for $[\text{Ni}(\text{PCy}_3)_2]_2(\text{N}_2)$ and $[\text{Ni}(\text{P}^i\text{Pr}_3)_2]_2(\text{N}_2)$, respectively [51]. Therefore, the structure containing P^iPr_3 is closer to a D_{2d} -like symmetry with the PNiP planes perpendicular to each other, which can enhance the overlap of the nickel d-orbital of π -symmetry with both $1\pi_g$ orbitals in the N_2 fragment.

Related to the trialkylphosphine complexes beginning with Tolman's report, Waterman and Hillhouse showed that the use of nickel(0) complexes with chelating phosphines are also competent for formation of nickel(0)–dinitrogen species [52]. They reported the use of a sterically hindered diphosphine, ${}^t\text{BuP}^t\text{BuP}$ (1,2-bis(di-*tert*-butylphosphino)ethane), which was previously demonstrated to afford η^2 adducts with benzene (Figure 8.3) [53]. Reaction of this precursor with N_2 in the presence of triphenylphosphine yielded a dark-red compound, $\text{Ni}({}^t\text{BuP}^t\text{BuP})(\text{PPh}_3)(\text{N}_2)$. In this compound, the nickel(0) center is held within a pseudotetrahedral environment with a terminal end-on N_2 ligand. The observed N–N bond distance is short (cf. $1.112(2)\text{ \AA}$ for free N_2), which is consistent with the other phosphine complexes (*vide supra*). However, the sterically demanding chelate and ancillary triphenylphosphine preclude the formation of the dinickel complexes, commonly obtained when smaller trialkylphosphines were used.

Even though the studies involving nickel(0/I) compounds with these mono- and bidentate phosphines date from 1970s or 1980s, it was not until that late 2000s that new families of nickel–dinitrogen compounds using more judiciously designed ligands were reported in the literature. Because of the large number of ligands of this type used for the synthesis of nickel–dinitrogen complexes, the next sections group similar ligand scaffolds in order to provide a better correlation with the synthesis and reactivity of these compounds.

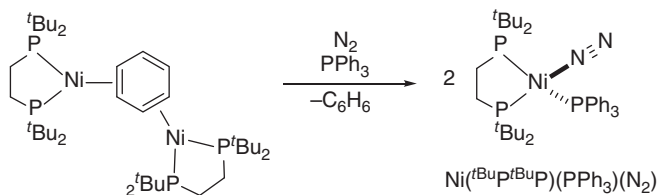


Figure 8.3 Synthesis of a nickel(0)–dinitrogen complex using chelating phosphines.

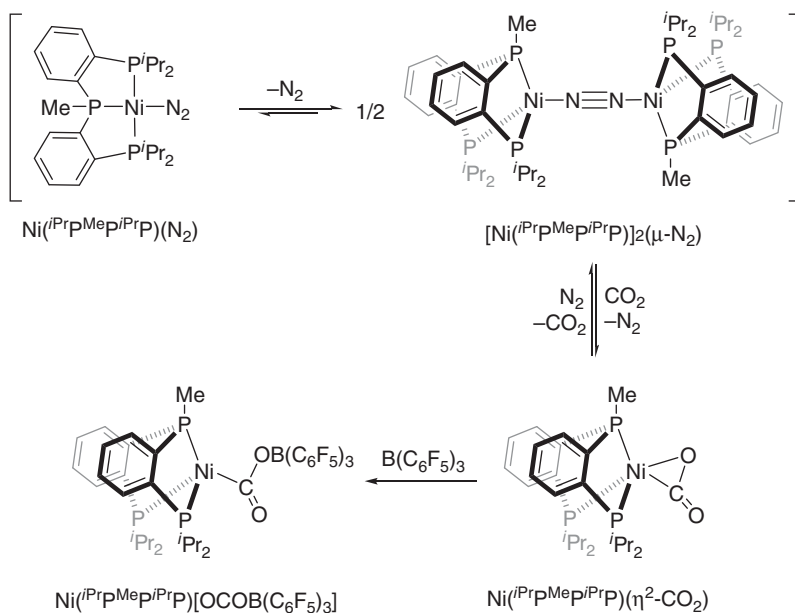


Figure 8.4 Synthesis of a nickel(0) dinitrogen complex using a phosphorous-based pincer ligand and its reactivity toward CO_2 .

Pincer Ligand Systems Relying on the σ donor ability of phosphine-based ligands, Kim et al. have accessed a nickel(0)–dinitrogen complex by employing a pincer ligand architecture ($i\text{PrP}^{\text{Me}}\text{P}^{\text{iPr}}\text{P}$) to support a zero-valent nickel center. The dinitrogen complex is readily formed by metalating the free pincer ligand with $\text{Ni}(\text{COD})_2$ (COD, 1,5-cyclooctadiene) under a dinitrogen atmosphere. In solution, this approach affords a dinickel(0)–dinitrogen complex, $[\text{Ni}(i\text{PrP}^{\text{Me}}\text{P}^{\text{iPr}}\text{P})]_2(\mu\text{-}1,2\text{-N}_2)$, which is in equilibrium with the monometallic species with a terminal end-on N_2 donor, $\text{Ni}(i\text{PrP}^{\text{Me}}\text{P}^{\text{iPr}}\text{P})(\text{N}_2)$ (Figure 8.4). The presence of the monometallic species was evidenced by an absorption at 2083 cm^{-1} in the infrared spectrum of a solution of the dinickel compound in benzene. The dinickel species gave rise to a peak in the Raman spectrum at 2042 cm^{-1} , showing that the coordination to the two nickel(0) centers resulted in further activation of the dinitrogen fragment. The structure of these compounds evidences a more scorpionate-like coordination mode of the pincer ligand, as opposed to a meridional ligation, thereby affording pseudotetrahedral nickel(0) centers. Exposure of these nickel–dinitrogen complexes to CO_2 results in N_2 loss and concomitant formation of a new nickel complex in which CO_2 is coordinated in a η^2 manner. Reversible interconversion between the N_2 and CO_2 adducts was observed, evidencing that both substrates are not strongly ligated to the nickel(0) center. The species containing the coordinated CO_2 could be trapped by the use of Lewis acids, such as $\text{B}(\text{C}_6\text{F}_5)_3$, resulting in a complex containing CO_2 in a η^1 coordination mode [54].

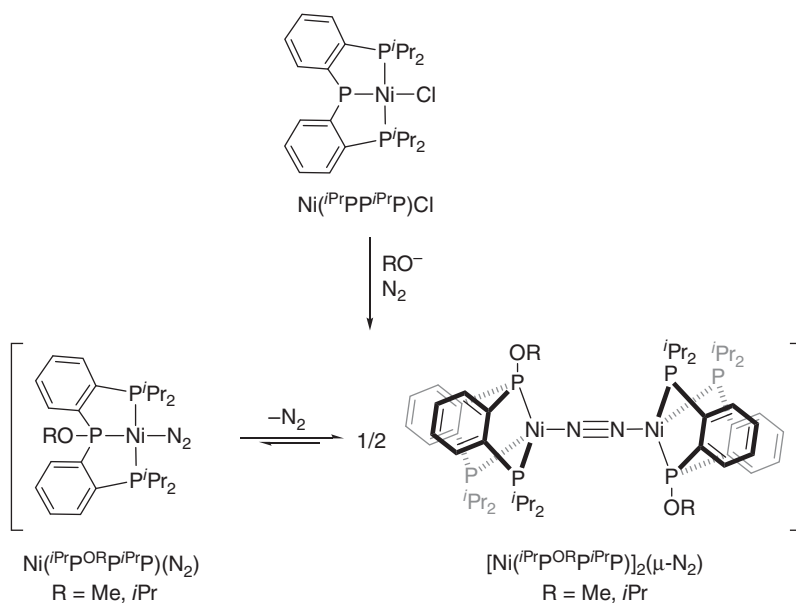


Figure 8.5 Synthesis of nickel(0)–dinitrogen complexes supported by phosphinite groups.

One advantage of molecular species is that the effect of specific attributes of the metal center (e.g. coordination number and ligand donor strength) on dinitrogen activation can be systematically studied. With this in mind, Kim et al. examined the chemistry of an analogous pincer ligand in which the central phosphine was replaced by a phosphide (Figure 8.5). Exposure of the square-planar nickel(II) methoxide complex to dinitrogen resulted in the transfer of the methoxide group to the central phosphide of the ligand, leading to a formal two-electron reduction of the nickel center and coordination of dinitrogen, forming dinickel complexes of the type $[\text{Ni}(\text{iPrP}^{\text{ORP}}\text{iPrP})]_2(\mu\text{-N}_2)$ [55–57]. Alkyl for alkoxide substitution on P donors diminishes σ donor strength and increases π -acidity; thus, comparison of the N–N bond distance between the phosphinite and the phosphine analogs could provide an insight into how ligand electronic effects tune N_2 at nickel(0). Surprisingly, the subtle change in donor properties here had a minimal effect on the extent of activation observed in these complexes, with the N–N bond distance in $[\text{Ni}(\text{iPrP}^{\text{ORP}}\text{iPrP})]_2(\mu\text{-N}_2)$ being 1.112(5) and 1.133(4) Å for R = Me and *iPr*, respectively, which is comparable to those observed for $[\text{Ni}(\text{iPrP}^{\text{Me}}\text{iPrP})]_2(\text{N}_2)$ (1.124(3) Å) [54].

As one might anticipate, more substantial variations to the above phosphorous-only pincer ligand have also been explored. In particular, substitution of the central PMe donor for a monoanionic Si–Me unit as well as introducing cyclohexyl substituents on the flanking phosphine arms affords the PSiP pincer ligand. Considering the vacant square-planar coordination site, this ligand provides a stronger trans influence vis-à-vis the PMe analog [58]. Suh and coworkers reported the nickel(II)–hydride complex of this ligand, which readily forms nickel(0) N_2 -bound species upon exposure to N_2 . Two products are observed,

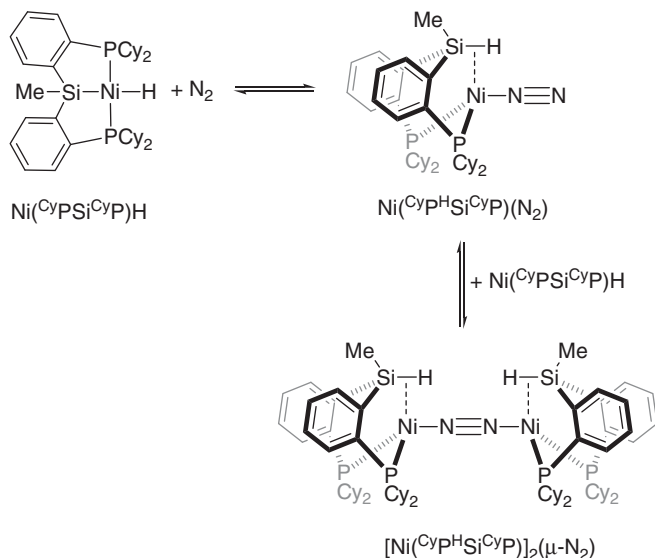


Figure 8.6 Formation of a dinitrogen adduct facilitated by the formation of a Si—H bond using a pincer ligand framework.

which are both analogous to the all phosphorus analogs: a monomeric terminal end-on complex and a (μ -1,2-dinitrogen)dinickel(0) species (Figure 8.6) [59]. Formation of these compounds is accompanied by a reductive coupling to produce a Si—H bond that is engaged in an agostic interaction with the nickel(0) centers. This reactivity is unusual for metal hydrides, which generally engage in the reductive elimination pathways or protonation to produce H_2 instead.

Relatedly, a similar agostic interaction, albeit B—C_{Ph} instead of Si—H, is also observed in a nickel(0)–dinitrogen complex of a ligand containing a central borane ($i^{\text{Pr}}\text{P}^{\text{Ph}}\text{B}^{i^{\text{Pr}}}\text{P}$). The starting nickel(I) bromide complex $\text{Ni}(i^{\text{Pr}}\text{P}^{\text{Ph}}\text{B}^{i^{\text{Pr}}}\text{P})\text{Br}$ was synthesized by a comproportionation approach metalating the ligand with equimolar amounts of $\text{Ni}(\text{cod})_2$ and NiBr_2 [60]. Reduction of this nickel(I) bromide using sodium mercury amalgam led to the formation of a nickel(0)–dinitrogen complex, for which the N—N distance was $\sim 1.10 \text{ \AA}$ and a $\nu_{\text{N-N}} = 2152 \text{ cm}^{-1}$ was observed. These values are consistent with minimal activation of N—N bond, which was further evidenced by the facile substitution of N_2 by other donors (e.g. H_2). Interestingly, no evidence of N_2 coordination was observed for the analogous complex in which the B and P substituents were mesityl and phenyl, respectively. This fact could be explained by the increased steric hindrance offered by the substituents in the ligand backbone [61].

In addition to the nickel(0)–dinitrogen complexes, pincer ligands have also allowed isolation of compounds in which dinitrogen coordinates to nickel(II) centers. For example, Connelly and collaborators demonstrated that the reaction of $[(\text{Et}_3\text{Si})_2\text{H}]^+$ with the nickel(II) chloride complex of a monoanionic PCP pincer ligand affords the cationic nickel(II)–($\eta^1\text{-N}_2$) complex (Figure 8.7) [62].

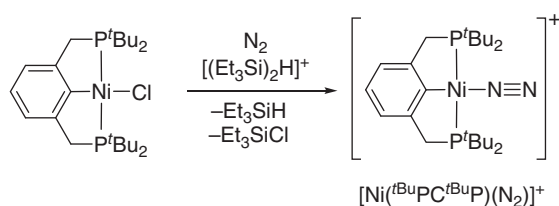


Figure 8.7 Synthesis of a nickel(II)-dinitrogen compound using a monoanionic PCP ligand.

Here, the steric protection afforded by the *tert*-butyl substituents and the judicious choice of solvent resulted in selective dinitrogen coordination to the open site after halide abstraction. Because a more electron-deficient metal center is present in this complex as compared to the nickel(0) compounds shown before, one would anticipate a lesser extent of π -backbonding and, consequently, a lower activation of the N_2 fragment reflected in shorter N–N bond distances. Indeed, the value for the N–N distance found in the crystal structure was 1.099 Å, which is very close to that for free dinitrogen (1.098 Å).

Although most of the examples of ligands showed so far are mostly phosphorous based, pincers containing not only phosphorous-based donor sites are also capable of stabilizing nickel(0) dinitrogen complexes. Zhu et al. recently published a 2,6-diiminepyridine ligand containing diisopropylphenyl groups at the imine nitrogen atoms ($\text{D}^{\text{iip}}\text{DIMPY}$) that support coordination compounds with low-valent metal centers [63]. Reduction of the nickel(II) bromide complex, $\text{Ni}(\text{D}^{\text{iip}}\text{DIMPY})\text{Br}_2$, with 2 equiv of NaH led to the formation of a square-planar nickel(0) dinitrogen complex. The crystallographic N–N distance in this complex is shorter than the N–N distance in free dinitrogen (1.097 Å), indicating minimal if any activation. The authors claim that a smaller distance for the bound N_2 could be an effect of either unaccounted disorder in the structure or an artifact because of nitrogen atom thermal motions. In spite of that, this compound showed an absorption at 2156 cm^{-1} in its infrared spectrum, indicating the activation of the dinitrogen fragment comparable to other Ni– N_2 species. One should note, however, that the oxidation state assignment for metal complexes of pyridine diimine ligands is uncertain as metal- vs. ligand-centered reductions are difficult to distinguish in these systems [64].

Pincer ligands describe a narrow subset of tridentate donors in which the ligand coordinates in a meridional manner. By definition then, the ferrocene-based triphosphine ligand (or FcPPP) pioneered by Cowie and collaborators is not explicitly a pincer. Given the similarity to the triphosphine pincer ligands, however, we include their system here [65]. Metalation of the FcPPP ligand with $\text{Ni}(\text{cod})_2$ under a N_2 atmosphere affords the corresponding nickel(0) complex as the end-on dinitrogen dinickel(0) complex, *rac*- $\{[\text{Ni}(\text{FcPPP})_2](\mu\text{-}1,2\text{-N}_2)\}$ (Figure 8.8). Substitution of one of the diphenylphosphine groups with a diphenylborane one (now called the FcPPB ligand) abrogates N_2 coordination, indicating that the ligand choice is crucial for the formation of such metal–dinitrogen compounds. Although the N–N distance of 1.122(3) Å obtained for *rac*- $\{[\text{Ni}(\text{FcPPP})_2](\mu\text{-}1,2\text{-N}_2)\}$ is comparable to the values obtained for the compounds previously discussed, this compound has an infrared absorption at 2006 cm^{-1} . This value is the lowest value observed for this class

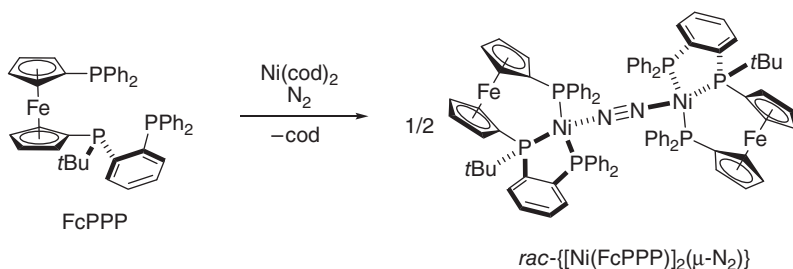


Figure 8.8 A tridentate phosphorous-based ligand that is able to coordinate nickel(0) centers to form adducts with N_2 .

of ligands, suggesting a relatively high degree of activation of the dinitrogen fragment.

Tetrapodal Phosphorous-Based Ligands Another class of ligands that readily supports nickel–dinitrogen adducts is the threefold symmetric triphosphine ligands pioneered by Peters. The initial design of these ligands leverage the relative energies of the metal frontier orbitals to favor metal–ligand multiple bonds. Recent generations of these ligands afford a tren-like coordination with a trigonal planar arrangement of P donor atoms and a unique axial donor atom (e.g. B, C, and Si). Metal complexes of these ligands have been applied to dinitrogen fixation – stoichiometric and catalytic – using exogenous electron and proton sources [66–74].

Although the iron complexes remain a significant focus considering the relevance to industrial and biological dinitrogen fixation, Peters and coworker reported that the reaction of nickel(II)-methyl compounds $\text{Ni}(\text{Si}^{\text{R}}\text{P}_3)(\text{CH}_3)$ ($\text{R} = i\text{Pr}$ and Ph) with proton sources led to the release of methane and consequent formation of nickel(II)–dinitrogen adducts, independent of the P substituent (Figure 8.9). Structural characterization of this series of complexes revealed a terminal end-on N_2 bound to a nickel(II) center in all cases; the diatomic ligand is minimally activated, and, in fact, the observed N–N distances are shorter than those in free N_2 . Vibrational spectroscopy supports this conclusion, with $\nu_{\text{N-N}} = 2223$ and 2234 cm^{-1} for $\text{R} = i\text{Pr}$ and Ph , respectively. These

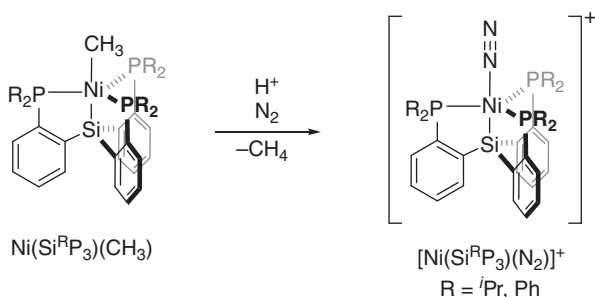


Figure 8.9 N_2 -bound nickel(II) compound formed using a tetrapodal phosphorous-based ligand architecture.

findings are consistent with primarily σ donation from the dinitrogen species and very poor π -backdonation from the metal [75]. Consistent with a weakly bound N_2 in the complexes $[Ni(Si^R P_3)(N_2)]^+$, exposing these species to other potential small-molecule ligands, such as carbon monoxide and acetonitrile, results in dinitrogen dissociation. Impressively, this cationic species also readily reacts with H_2 forming a thermally stable nickel(II)-dihydrogen complex.

In order to evaluate the effect of the axial donor on dinitrogen binding to nickel(II) in this ligand type, a similar synthetic approach was used to access the $[Ni(B^{iPr}P_3)]$ analog [76]. Unlike the cationic Si variant, the neutral nickel boratrane did not produce stable N_2 adducts, evidencing that the more electron-withdrawing borane was able to produce a more electron-poor metal center. The lack of substantial electron density around the nickel(II) site limits π -backdonation to the N_2 fragment, a factor that explains the ready loss of dinitrogen from metal complexes of this ligand [75].

Recently, Cammarota and Lu reported of a double-decker system that supports an indium(III)-nickel(0) dimetallic as shown in Figure 8.10 [77]. This system bears analogy to Peters' ligands mentioned above, with the benefit of facile substitution of the donor atom – In(III) here – across both transition metals and p-block elements. As a consequence, these double-decker ligands provide a unique opportunity to interrogate the distal atom's effect on the electronic structure of the reactive metal ion. The purple $Ni(N_4 In^{iPr} P_3)$ complex is readily formed by the combination of the In(III) complex with $Ni(cod)_2$ in tetrahydrofuran (THF) under argon. Exposure of this complex to N_2 leads to a color change to dark-red resulting from N_2 coordination in a terminal end-on mode. The nickel(0)-dinitrogen complex $Ni(N_4 In^{iPr} P_3)(N_2)$ is thermally stable with $\nu_{N-N} = 2144\text{ cm}^{-1}$ and even with the application of vacuum for extended periods. Analogs in which the distal metal was either Al(III) and Ga(III) were also reported, but N_2 coordination was not observed. These results highlight the subtle tuning afforded by the axial donor atom in this ligand set [78]. In this case, structural changes also accompany the choice of group 13 metal ions, which make separating influence of the electronic factors (viz the better overlap expected for In(III) with nickel(0) as compared with the lighter congeners) and structural effects (viz Ni(0) is displaced above the P_3 plane because of a larger In(III) radius vs. the Al(III) and Ga(III) compounds). The former (electronic effects) is anticipated to generate a more electropositive nickel center and favor dinitrogen coordination, whereas the latter

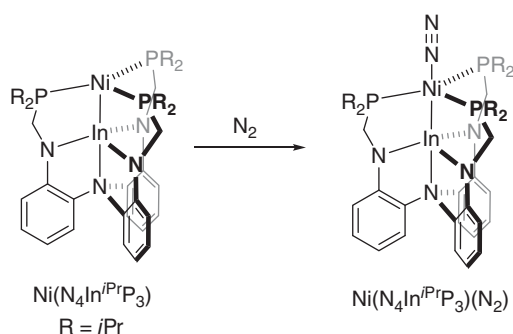


Figure 8.10 Spontaneous formation of a nickel(0)-dinitrogen complex using a double-decker system showing a Ni–In interaction.

leads to a more exposed and accessible nickel center. Similar to $[\text{Ni}(\text{Si}^{\text{R}}\text{P}_3)(\text{N}_2)]^+$, N_2 is released upon exposure of $\text{Ni}(\text{N}_4\text{In}^{\text{iPr}}\text{P}_3)(\text{N}_2)$ to H_2 , affording a dihydrogen adduct. However, the reactivity of this $\text{Ni}(\text{N}_4\text{In}^{\text{iPr}}\text{P}_3)(\text{H}_2)$ differs significantly from that of $[\text{Ni}(\text{Si}^{\text{R}}\text{P}_3)(\text{H}_2)]^+$.

β -diketiminate Ligand Scaffolds In addition to phosphorous-based ligands, β -diketiminate ligands are also known to be good σ donors and stabilize low-valent electron-rich metal centers, which are essential factors for the coordination and activation of N_2 as discussed in the previous sections.

Pfirrmann et al. reported in 2009 the first nickel(I)–dinitrogen complex employing supporting ligands of this type [79]. The β -diketiminate ligand (abbreviated $^{\text{tBu,iPr}}\text{NacNac}$) in which *tert*-butyl and 2,5-diisopropylphenyl groups are the substituents on the imine C and N atoms, respectively, enforces sufficient steric constraints around the metal center to ensure the formation of low-coordinate metal compounds. Reaction of the three-coordinate nickel(II) bromide complex of this ligand, $\text{Ni}(^{\text{tBu,iPr}}\text{NacNac})\text{Br}$, with 2 equiv of potassium triethylborohydride (KBHET_3) generates a dark-red dinickel(I) compound, $[\text{Ni}(^{\text{tBu,iPr}}\text{NacNac})]_2(\mu\text{-}1,2\text{-N}_2)$, in which the metal centers are bridged in a linear manner by a N_2 molecule (Figure 8.11). The proposed mechanism for this reaction involves an intermediate dihydride complex, which reductively eliminates H_2 to generate a low-valent nickel species that ultimately coordinates

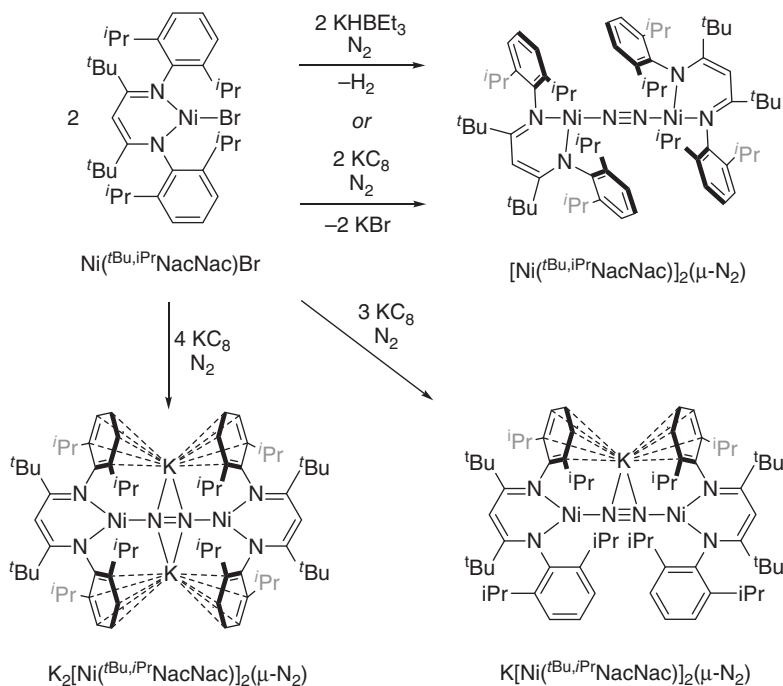


Figure 8.11 Formation of nickel(I)–dinitrogen complexes bearing a β -diketiminate ligand and the stepwise reduction of the N_2 fragment.

dinitrogen. Consistent with a low-valent nickel intermediate, the dinitrogen adduct could also be obtained by the reduction of $\text{Ni}(\text{}^t\text{Bu},i\text{PrNacNac})\text{Br}$ with 1 equiv of potassium graphite (KC_8).

The electrochemical data suggested that $[\text{Ni}(\text{}^t\text{Bu},i\text{PrNacNac})]_2(\mu\text{-}1,2\text{-N}_2)$ could be further reduced, conceivably generating either the dinickel(0)–dinitrogen complex or a formally diazenido–dinickel(I) species. When $\text{Ni}(\text{}^t\text{Bu},i\text{PrNacNac})\text{Br}$ was exposed to 1.65 or 2.30 equiv of KC_8 , two new products were obtained showing $[\text{Ni}_2(\mu\text{-N}_2)]^+$ and $[\text{Ni}_2(\mu\text{-N}_2)]^0$ cores (Figure 8.11), respectively. Potassium cations are incorporated in both complexes, interacting with the N_2 fragment in a side-on manner and with the π -cloud in the diisopropylphenyl substituents. The bond metrics and vibrational data support a stepwise reduction of the N_2 fragment in lieu of metal-centered reduction. Specifically, the N–N bond distances of 1.14 and 1.19 Å for the $[\text{Ni}_2(\mu\text{-N}_2)]^+$ and $[\text{Ni}_2(\mu\text{-N}_2)]^0$ clusters, respectively, are progressively longer than the 1.120 Å distance in $[\text{Ni}(\text{}^t\text{Bu},i\text{PrNacNac})]_2(\mu\text{-}1,2\text{-N}_2)$. The energies for $\nu_{\text{N-N}}$ also decrease systematically with decreasing charge of the $[\text{Ni}_2(\mu\text{-N}_2)]^{2+/1+/0}$ core from 2164 to 1825 to 1696 cm^{-1} , respectively. In addition, density functional theory (DFT) calculations support a negative charge buildup on the dinitrogen fragment with further reduction.

More recently, Horn et al. demonstrated the stepwise reduction of the initial dinitrogen adduct, $[\text{Ni}(\text{}^t\text{Bu},i\text{PrNacNac})]_2(\mu\text{-}1,2\text{-N}_2)$, by controlled addition of alkali reducing agent [80]. By using KC_8 or sodium sand or combinations thereof, the two-electron reduced compounds with varying ratios of K^+ and Na^+ , $\text{Na}_2[\text{Ni}(\text{}^t\text{Bu},i\text{PrNacNac})]_2(\mu\text{-N}_2)$ and $\text{KNa}[\text{Ni}(\text{}^t\text{Bu},i\text{PrNacNac})]_2(\mu\text{-N}_2)$, were accessible. From the structural and spectroscopic data on these compounds, it was evident that the identity of the alkali cation minimally influenced the extent of the activation of dinitrogen because these compounds show similar N–N bond distances when compared to $\text{K}_2[\text{Ni}(\text{}^t\text{Bu},i\text{PrNacNac})]_2(\mu\text{-N}_2)$. However, the alkali cations likely result in a similar push–pull effect as observed in Jonas’s lithium– and sodium–nickel compounds [39, 41]. Computational studies by Cundari and coworkers on the analogous low-valent iron systems are consistent with the alkali cations enhancing N_2 activation [81].

In terms of reactivity, the doubly reduced compound $\text{K}_2[\text{Ni}(\text{}^t\text{Bu},i\text{PrNacNac})]_2(\mu\text{-}1,2\text{-N}_2)$ reacts upon exposure to CO to afford the nickel(0)–carbonyl complex, $\text{K}_2[\text{Ni}(\text{}^t\text{Bu},i\text{PrNacNac})(\text{CO})]_2$ (Figure 8.12). This result is surprising as it implies a formal reduction of the nickel(I) centers to nickel(0) by activated N_2 fragment, highlighting the reversible redox properties of activated dinitrogen ligands [80, 82]. Indeed, the nitride to dinitrogen conversion with concomitant metal reduction reported by Holland and coworkers further emphasizes this trend. Further downstream reactivity of the carbonyl complex includes methylation with CH_3I to generate a nickel–acyl in which the acetyl group was coordinated in a η^2 manner. This resultant nickel(0)–acetyl complex reacts with thiophenol to liberate the thioester, mimicking the activity of acetyl coenzyme A synthase.

Holze et al. also reported that the doubly reduced complex, $\text{K}_2[\text{Ni}(\text{}^t\text{Bu},i\text{PrNacNac})]_2(\mu\text{-N}_2)$, reacts with SF_6 – an extremely inert and highly potent greenhouse gas – to afford a three-coordinate nickel(I) fluoride complex and a (μ -sulfido)dinickel(I) species [83]. The latter is a rare example of an almost linear μ -sulfide bridging two nickel(I) centers (Figure 8.12).

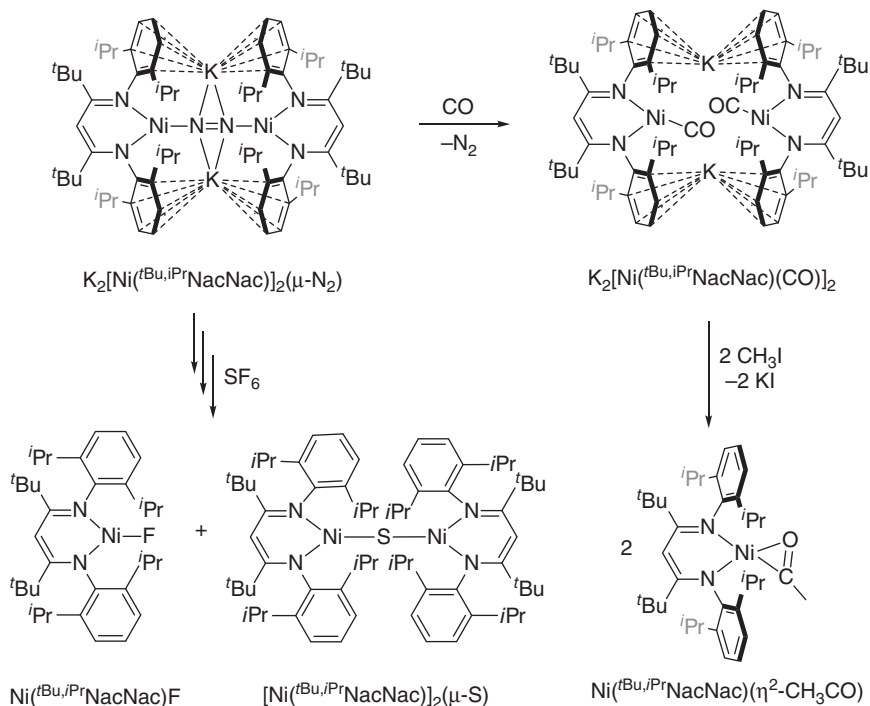


Figure 8.12 Reactivity of the doubly reduced nickel(I)–dinitrogen complex with a NaCNac ligand.

In addition to discrete compounds containing metallic nickel, Chavan et al. were able to evaluate the interaction of N_2 with open nickel(II) sites in a metal–organic framework (MOF) [84]. This material, called CPO-27-Ni, is a microporous coordination polymer derived from 2,5-dihydroxyterephthalate and nickel(II) centers. The resulting extended solid is a honeycomb lattice with hexagonal channels and one-dimensional chains of nickel cations at the channel vertices [85]. Removal of solvent molecules from this porous material produces an open coordination site on each nickel(II) ion at which several small molecules (e.g. H_2 , CH_4 , CO_2 , and NO) readily bind (Figure 8.13) [86–90]. More interesting to the scope of this discussion, the authors reported that the adsorption enthalpy of N_2 is -17 kJ mol^{-1} at the five-coordinate nickel(II) sites, which agrees with a weak interaction as compared to other substrates, such as CO or NO (-50 and

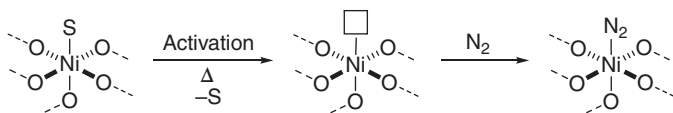


Figure 8.13 Representation of a single nickel(II) site in CPO-27-Ni. The parent framework contains solvent molecules (S) coordinated with the nickel(II) sites that can be released by activation under high temperatures to produce coordinatively unsaturated centers that can bind to N_2 .

–90 kJ mol⁻¹, respectively). Here, N₂ is proposed to bind in a linear end-on η¹ manner based on the IR absorption data. Consistent with the expected poor backbonding from Ni(II) to the bound N₂, the N–N stretching vibrations for the Ni-bound N₂ in CPO-27-Ni range from 2341 to 2334 cm⁻¹, only 18–25 cm⁻¹ different from gaseous N₂.

8.2.1.4 Structural Relationships and Comparisons

As we can observe in Table 8.1, most of the nickel–dinitrogen species have minimal activation of the N₂ fragment because the values for the N–N bond distance and the energy of the N₂ stretching vibration are close to the reported values for free N₂ (viz N–N bond distance of 1.10 Å and ν_{N–N} of 2359 cm⁻¹ in free N₂) [1, 42]. Three families of compounds demonstrate substantial activation: Beck's bis(triisopropylphosphine)nickel(0) compound, the reduced β-diketimate nickel compounds from Limberg and coworkers, and the Jonas's complexes supported by nickel and alkali phenyl groups.

The dinickel(0) dinitrogen complex, [Ni(PiPr₃)₂]₂(μ-N₂), reported by Beck and collaborators is atypical among all other nickel phosphine complexes. At

Table 8.1 Structural data for the nickel–dinitrogen complexes: N–N bond distances and N–N stretching vibrational mode absorption energies (ν_{N–N}).

| Compound | N–N distance (Å) | ν _{N–N} (cm ⁻¹) | References |
|--|---------------------|--|------------|
| Ni(N ₂) | 1.14 ^a) | 2089.4 ^b) | [31, 37] |
| Ni(N ₂) ₂ | 1.10 ^a) | 2104.8 ^b) | [32] |
| Ni(N ₂) ₃ | n.r. | 2136.7 ^b) | [32] |
| Ni(N ₂) ₄ | n.r. | 2171.4 ^b), 2183.3 ^b), 2251.1 ^c) | [33] |
| NiCl(N ₂) | n.r. | 2246.1 ^b) | [37] |
| NiCl ₂ (N ₂) | n.r. | 2260.3 ^b), 2280.9 ^b) | [38] |
| NiBr ₂ (N ₂) ₂ | n.r. | 2261.4 ^b), 2281.4 ^b) | [38] |
| Ni(CO) ₃ (N ₂) | n.r. | 2267 ^b) | [36] |
| C ₆ H ₅ [Na(Et) ₂] ₂ [(C ₆ H ₅) ₂ Ni] ₂ N ₂ | 1.359(18) | n.r. | [41] |
| NaLi ₆ (OEt) ₄ (OEt) ₂ | | | |
| [(C ₆ H ₅ Li) ₆ Ni ₂ N ₂ (Et ₂ O) ₂] ₂ | 1.35 | n.r. | [40] |
| Ni(PET ₃) ₃ (N ₂) | n.r. | 2063, 2070, 2074 | [44, 47] |
| Ni(PET ₂ Ph) ₃ (N ₂) | n.r. | 2065 | [47] |
| Ni(PnBu ₃) ₃ (N ₂) | n.r. | 2060, 2063 | [47] |
| [Ni(PCy ₃) ₂] ₂ (N ₂) | 1.12 | n.r. | [46] |
| [Ni(PCy ₃) ₂](N ₂) | n.r. | 2028 | [46] |
| [Ni(PiPr ₃) ₂] ₂ (μ-N ₂) | 1.158(5) | 1908 ^c) | [50] |
| Ni(^t BuP ^t BuP)(N ₂)(PPh ₃) | 1.112(2) | 2072 | [52] |
| Ni(ⁱ PrP ^{Me} P ⁱ PrP)(N ₂) | n.r. | 2083 | [54] |

(Continued)

Table 8.1 (Continued)

| Compound | N–N distance (Å) | $\nu_{\text{N-N}}$ (cm ⁻¹) | References |
|--|--------------------|--|------------|
| [Ni(ⁱ PrP ^{Me} P ⁱ PrP)] ₂ (μ-N ₂) | 1.124(3) | 2042 ^c , 2045 ^c | [54] |
| [Ni(ⁱ PrP ^O iPrP ⁱ PrP)] ₂ (μ-N ₂) | 1.133(4) | n.r. | [56] |
| [Ni(ⁱ PrP ^{OMe} P ⁱ PrP)] ₂ (μ-N ₂) | 1.112(5) | 2038 ^c | [55] |
| Ni(ⁱ PrP ^{OMe} P ⁱ PrP)(N ₂) | n.r. | 2094 | [55] |
| Ni(^{Cy} P ^H Si ^{Cy} P)(N ₂) | 1.110 ^c | 2150 | [59] |
| [Ni(^{Cy} P ^H Si ^{Cy} P)] ₂ (μ-N ₂) | 1.127(3) | 2050 | [59] |
| Ni(^{Dii} P ^{DIMPY})(N ₂) | 0.92 ^d | 2156 | [63] |
| [Ni(^t BuPC ^t BuP)(N ₂)] [B(C ₆ F ₅) ₄] | 1.099 | n.r. | [62] |
| [Ni(^{Mes} DPBPh)(N ₂)] | 1.101(2), 1.102(2) | 2152 | [60] |
| <i>rac</i> -{[Ni(EcPPP)] ₂ (μ-N ₂)} | 1.122(3) | 2006 | [65] |
| [Ni(Si ⁱ PrP ₃)(N ₂)] ⁺ | 1.087(2) | 2223 | [75] |
| [Ni(Si ^{Ph} P ₃)(N ₂)] ⁺ | 1.083(3) | 2234 | [75] |
| Ni(N ₄ In ⁱ PrP ₃)(N ₂) | 1.103(5) | 2144 | [77] |
| [Ni(^t Bu, ⁱ PrNacNac)] ₂ (μ-N ₂) | 1.120(4) | 2164 | [79] |
| K[Ni(^t Bu, ⁱ PrNacNac)] ₂ (μ-N ₂) | 1.143(8) | 1825 ^c | [79] |
| Na ₂ [Ni(^t Bu, ⁱ PrNacNac)] ₂ (μ-N ₂) | 1.192(3) | 1685 ^c | [80] |
| KNa[Ni(^t Bu, ⁱ PrNacNac)] ₂ (μ-N ₂) | 1.195(4) | 1689 ^c | [80] |
| K ₂ [Ni(^t Bu, ⁱ PrNacNac)] ₂ (μ-N ₂) | 1.185(8) | 1696 ^c | [79] |

a) Result from DFT calculations.

b) Obtained in a solid inert gas matrix between 10 and 25 K using ¹⁴N₂.

c) Result from Raman spectra.

d) Authors concluded that this distance is a result from artifacts or disorder.

n.r., not reported.

1908 cm⁻¹, the N–N stretching frequency for this complex is the lowest reported among this family and more than 100 cm⁻¹ lower in energy than the closest system [50]. Although there were no detailed studies on the reasons of this further activation, the authors suggested the ligand sterics allow for close approach of the two nickel ions – evidenced by the Ni–Ni distances of ~4.7 Å – as well as near D_{2d} symmetry, which provides an enhanced overlap with the orthogonal π* orbitals on N₂. Thus, correlating the role of ligand effects on nickel–dinitrogen orbital overlap in a relatively simple system could provide valuable insights into developing nickel catalysts for N₂ activation and functionalization.

The other two families of compounds that are a departure from the otherwise minimal activation of the dinitrogen donor are those in which alkali cation(s) are in close proximity to the N₂ ligand. The β-diketimate compounds of the type AB[Ni(^tBu,ⁱPrNacNac)]₂(μ-N₂) (A = K, B = K, Na) exhibit substantial activation of the N₂ fragment, arising from a ligand-centered reduction as compared to a metal centered one. This shift toward directed N₂ reduction is likely enhanced by the close association of the charge-balancing alkali cations with the increasing negative charge of the dinitrogen donor [79, 80].

Similarly, the phenyl–lithium and –sodium adducts reported by Jonas were one of the first reports of nickel–dinitrogen complexes with N_2 –alkali interactions. In contrast to the end-on coordination of dinitrogen in the Limberg complexes, these compounds combine the benefits of both alkali cation association and a side-on $\mu\text{-}\eta^2\text{:}\eta^2$ coordination mode for N_2 [39–41]. Although vibrational data are not reported for these compounds, the N–N bond distances are the longest of any nickel–dinitrogen complex to date. Specifically, the reported distances are intermediate with respect to the common values for diazenide and hydrazide ligands in metal complexes, suggesting substantial charge transfer into the dinitrogen ligand [42]. An important observation from these alkali–cation complexes is that the identity of the alkali cation does not dramatically influence the degree of activation, with similar structural parameters for the interaction with K or Na [80].

8.2.2 Palladium and Platinum

As compared to nickel, isolable complexes in which N_2 is coordinated to palladium and platinum centers remain unknown. Hitherto, all known examples arise from low-molecular-weight species produced by laser ablation of solid matrices and subsequent trapping of reactive species at low temperatures in a similar way as shown for the matrix-assisted nickel–dinitrogen species discussed in Section 8.2.1.2.

The earliest examples of matrix-assisted species date from the 1970s. These studies involve the formation of binary compounds of the type $Pd(N_2)_n$ and $Pt(N_2)_n$, with $n = 1\text{--}3$ [25, 27, 91–96]. The palladium compounds showed absorptions in the range $2210\text{--}2240\text{ cm}^{-1}$ and the platinum analogs in the range $2170\text{--}2210\text{ cm}^{-1}$, indicating that platinum(0) led to a better activation of the N–N bond.

More recently, Souvi et al. observed the formation of dipalladium species by the cocondensation of Pd- and N_2 -effusive beams in neon and argon matrices [96]. In these studies, three isomeric $Pd_2(N_2)$ species were identified by infrared spectroscopy in which N_2 is coordinated to the metal–metal-bonded Pd_2 unit in a cis- $\mu\text{-}1,2$ mode, a $\mu\text{-}1,1$ mode, and a terminal coordination to only one of the Pd centers. The corresponding N–N stretching vibrations were observed at 1823, 1990, and 2178 cm^{-1} , respectively. A fourth isomer with no Pd–Pd interactions was also found and proposed as a linear ($\mu\text{-}1,2$ -dinitrogen)dipalladium(0) species, with a N–N stretching vibration of 2141 cm^{-1} . Interestingly, Citra et al. observed the comparable linear species for a $Pt_2(N_2)$ species, indicating a possible coordination mode preference for group 10 metals, which agrees with the extensive number of complexes with a linear Ni–N \equiv N–Ni fragments (Section 8.2.1.2) [95].

Beyond these reports of binary compounds of palladium or platinum with dinitrogen, Ozin and Klotzbücher in 1975 also reported the identification of species of the type $Pd(O_2)(N_2)_n$ and $Pt(O_2)(N_2)_n$ ($n = 1, 2$) using infrared spectroscopy [97]. In those species, the authors concluded that O_2 binds in a side-on manner, whereas N_2 binds in an end-on mode, which is the most common coordination mode for metal–dinitrogen complexes. The N_2 fragment in these

complexes was minimally activated as compared to the binary compounds of the type $M(N_2)_n$ ($M = Pd, Pt, n = 1-3$). This difference was rationalized as greater π -backbonding into the O_2 ligand. Consistently, vibrational data support significant superoxide or peroxide character for the O_2 donor and affords more electron-deficient metal centers. More recent studies have identified cationic species $[Pt(NH_3)_2(N_2)X]^+$ with $X = OH$ or Cl . These ions were observed in high-resolution electrospray mass spectrometry experiments for the study of the hydrolysis of cisplatin, *cis*- $Pt(NH_3)_2Cl_2$ [98, 99].

8.3 Group 11 Transition Metal–Dinitrogen Complexes

As compared to the growing coordination chemistry of dinitrogen to group 10 metals, the chemistry of the coinage metals and N_2 remains poorly understood as dinitrogen adducts of these metals remain elusive.

In the following sections, the reported compounds of copper, silver, and gold containing N_2 will be discussed with the focus on their syntheses and structure.

8.3.1 Copper

The initial forays into the coordination of dinitrogen to copper centers were in the 1990s and resulted from studies on copper-doped extended solids, such as copper ion-exchanged mordenite and Cu-ZSM-5 [100–103]. These materials have applications as catalysts for methane-to-methanol conversion, and gas adsorption coupled to vibrational methods provided molecular insights into copper–substrate interactions. Dinitrogen adsorption isotherms and infrared measurements evidenced the coordination of N_2 in an end-on manner to accessible copper(I) coordination sites with enhanced heats of adsorption for N_2 physisorption ($50-75 \text{ kJ mol}^{-1}$) vs. the parent material. Experiments stemming from this early work identified $[Cu_2O]^{2+}$ sites – formed upon treating Cu-ZSM-5 with N_2O , O_2 , or NO_x species – as the catalytically active species for the oxidation of hydrocarbons including methane [104–107]. The interaction of N_2 molecules to copper metal was also studied by Zeppenfeld et al. where they demonstrated a pinwheel arrangement of adsorbed N_2 molecules on the Cu(110) surface. The calculated binding energy for N_2 on this surface was approximately -11 kJ mol^{-1} , consistent with a weak interaction governed by dispersion forces [108]. Moving from solid surfaces to more discrete systems, N_2 adsorption on small cationic copper clusters (Cu_n^+) was investigated by Ohshimo et al. They evaluated the physisorption of N_2 molecules in clusters ranging the nuclearity from 2 to 17 and observed a negative correlation between N_2 binding energy and cluster nuclearity ($n \leq 6$), in accordance with DFT calculations [109].

8.3.1.1 Matrix-Assisted Isolation of Binary or Ternary Compounds

As mentioned in Section 8.2.1.2, there are an extensive number of studies exploring the laser ablation of metal salts or compounds and isolation of reactive species under controlled conditions.

Following this approach, Chen et al. in the 2000s used copper(II) halides as targets for 1064-nm laser ablation in the presence of a gas mixture containing 0.5% of N_2 in argon, with the resulting species characterized by infrared spectroscopy after isolation in a solid Ar matrix at 11 K [37]. The products were assigned as the ternary complexes $CuCl(N_2)$ and $CuBr(N_2)$ when $CuCl_2$ and $CuBr_2$ were used as targets, respectively. New infrared absorptions at $\sim 2297\text{ cm}^{-1}$ were reported for both dinitrogen compounds, with these absorptions attributed to a N–N stretching mode. The analogous experiment using $CuCl$ instead of $CuCl_2$ afforded a product with an IR absorption at the same energy as that observed for $CuCl_2$ as the target, indicating that the copper dinitrogen interaction is minimally influenced by the formal oxidation state of copper. Use of isotopically labeled N_2 ($^{15}N_2$ and ^{14}N – ^{15}N) supported inequivalent in these $Cu(N_2)$ species, excluding side-on dinitrogen coordination. Thus, the model proposed a linear structure containing a terminal end-on N_2 coordination with minimal, if any, activation of the dinitrogen fragment. DFT calculations performed on the proposed geometries are consistent with this model. A similar linear X – Cu – $N\equiv N$ species was also observed in the rotational spectroscopy studies for the laser ablation of copper metal in the presence of N_2 and SF_6 . The resulting $FCu(N_2)$ species also exhibits little activation of the $N\equiv N$ bond, consistent with DFT results and data on the other halides [110].

With a similar experimental apparatus for 1064-nm laser ablation, Elustondo et al. showed that the use of neat N_2 instead of diluted N_2 in Ar allows isolation of higher nuclearity clusters. Through a combined experimental and theoretical approach, the products were confirmed as two dicopper species: $Cu_2(N_2)$ and $Cu_2(N_2)_2$. In both cases, the N_2 ligands are proposed to adopt a terminal end-on coordination mode [111]. Both species also show limited activation of the N–N bond, with calculated N–N bond distances of c. 1.10 \AA and experimentally-observed N–N stretching modes at $\sim 2280\text{ cm}^{-1}$. In addition, the presence of small amounts of CO in the gas mixture was demonstrated to limit formation of the dicopper–dinitrogen species, generating mononuclear copper species with both CO and N_2 ligands. In contrast to the nickel system, coordination of π -acidic CO to the copper atoms resulted in an increase in the N_2 binding energy.

In a related report, Lu and Xu were studying the interactions of copper atoms in the mixtures of carbon monoxide and dinitrogen in excess argon. Consistent with the CO studies by Elustono et al., $Cu(CO)(N_2)$ and $Cu(CO)(N_2)_2$ were among the observed products along with copper carbonyl species [112]. DFT calculations reproduce the vibrational data for models in which N_2 is bound in a linear η^1 manner; the optimized structures for $Cu(CO)(N_2)$ and $Cu(CO)(N_2)_2$ are best described as linear and trigonal planar around the copper center, respectively, with N–N bond distances of $\sim 1.12\text{ \AA}$. Both compounds have absorptions at $\sim 2070\text{ cm}^{-1}$, which is significantly lower than other binary or ternary compounds obtained by matrix-assisted isolation. This greater extent of N_2 activation is attributed to a change in electronic structure of the copper atoms upon coordination to CO, favoring the π -backdonation to both N_2 and CO.

These studies provide clear evidence that the supporting ligands around the copper center can dramatically tune the strength of the interaction between N_2 and the metal center.

8.3.1.2 Coordination Compounds

The first copper coordination compound in which $Cu-N_2$ was observed and structurally characterized was reported by Murray et al. in 2014 [113]. Deprotonation of a trinucleating tris(β -diketimine) cyclophane ligand, $H_3L^{Et/Me}$, with benzylpotassium (BnK) in THF, followed by metalation with the benzene adduct of copper(I) triflate under a dinitrogen atmosphere affords the tricopper(I)–dinitrogen complex as a dark-red complex (Figure 8.14). This color sharply contrasts the pale yellow–green of the related monoanionic (μ_3 -chloro)tricopper(I) complex, suggesting that the intense visible absorption of the dinitrogen complex may be a copper-to-dinitrogen charge transfer [114].

Crystals suitable for structural determination were obtained by slow evaporation of a THF solution of the red compound and confirmed tricopper(I) complex bound to N_2 , with a formula of $Cu_3(N_2)L^{Et/Me}$. The N_2 ligand is positionally disordered in the structure with a major component (accounting for 75%) having a N–N distance of 1.0956(1) Å and η^1 coordination to two of the copper(I) centers and η^2 coordination to the remaining copper(I) (i.e. a μ - η^1 : η^2 : η^1 -dinitrogen), which is the mode represented in Figure 8.14. The minor component (representing 25%) contains a N_2 fragment with a N–N distance of 1.0854(1) Å, and all of the copper(I) atoms are coordinated by a η^1 coordination mode, with one dinitrogen N atom as a μ -1,1 bridging ligand and the other adopting a μ -1,2 mode.

This $Cu_3(N_2)L^{Et/Me}$ complex has an isotopically sensitive feature at 1952 cm^{-1} in the resonance Raman spectrum, indicating a relatively activated dinitrogen fragment when compared to other group 10 and 11 metal–dinitrogen complexes. DFT calculations primarily suggest dispersion interactions between the metal centers in the N_2 fragment, which appears inconsistent with the ν_{N-N} mode lying $\sim 400\text{ cm}^{-1}$ lower in energy than in the free diatomic. Minor structural changes were noted to dramatically influence the calculated energy for this vibration, implying that subtle changes to the interactions between the ancillary ligand(s) and the copper cations can significantly influence the extent of N_2 activation.

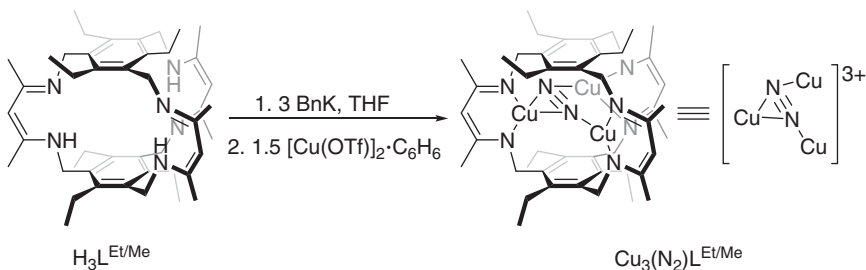


Figure 8.14 Use of a trinucleating cyclophane-type ligand for the formation of a tricopper(I)–dinitrogen adduct.

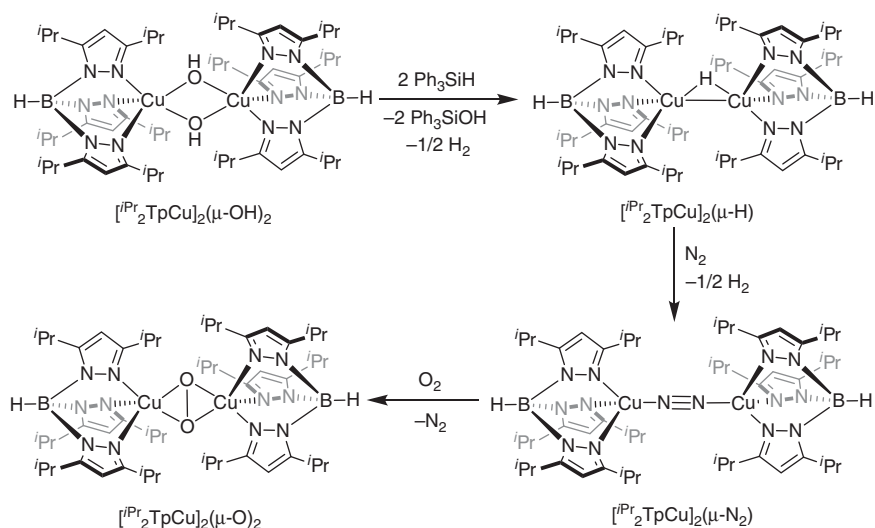


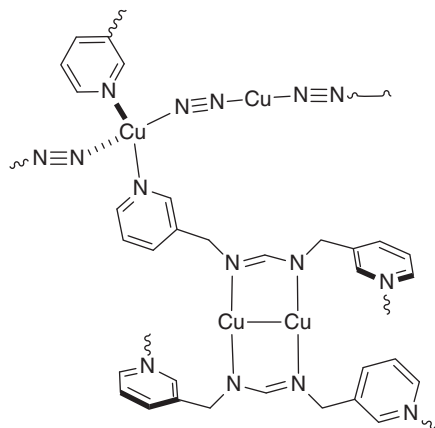
Figure 8.15 Synthesis of a dicopper dinitrogen adduct from copper(I) tris(pyrazolyl)borate (Tp) complexes.

In a more recent publication, Zhang et al. showed that a tris(pyrazolyl)borate (^RTp) ligand stabilizes low-coordinate copper(I) centers and, consequently, can lead to a copper(I)–dinitrogen species. Reaction of the di-(μ -hydroxo)dicopper(I) complex $[\text{iPr}_2\text{TpCu}]_2(\mu\text{-OH})_2$ with triphenylsilane (Ph_3SiH) affords a μ -hydrido-dicopper(I) species. Subsequent loss of H_2 from 2 equiv of this dimetallic followed by coordination to N_2 generates a complex containing a N_2 molecule coordinated to two copper(I) centers in an end-on manner ($[\text{iPr}_2\text{TpCu}]_2(\mu\text{-1,2-N}_2)$, Figure 8.15) [115]. As expected a N–N stretching vibration mode was observed at 2130 cm^{-1} and crystallographic N–N distances around 1.11 \AA , which agrees with a low degree of activation of the dinitrogen fragment.

The reaction of this dinuclear compound with acetonitrile or isonitriles generated the respective mononuclear copper(I) adducts with the release of N_2 , showing that the coordinating species can break the dimer and replace the dinitrogen fragment. These results also agree with the minimal N_2 activation conferred by this system. Also, when $[\text{iPr}_2\text{TpCu}]_2(\mu\text{-N}_2)$ was exposed to O_2 , N_2 was also released, and a dimeric di(μ -oxo) species $[\text{iPr}_2\text{TpCu}]_2(\mu\text{-O})_2$ was formed.

Another recent example of copper–dinitrogen coordination compounds was obtained by Hsu et al. in 2016. In their report, the solvothermal reaction of 3- and 4-(aminomethyl)-pyridine with triethyl orthoformate and copper(II) acetate in N_2 -saturated methanol generates two coordination polymers – depending on the substitution pattern of the pyridine employed – in which copper–dinitrogen interactions are integral to the network [116]. Prior work demonstrated that the mixtures of aminomethyl-pyridines and triethyl orthoformate in the presence of divalent copper salts lead to formamidinate ligands *in situ*, which act as the building blocks for the polymer network [117]. Use of N_2 -saturated methanol and 3-(aminomethyl)-pyridine afforded the expected deprotonated form of

Figure 8.16 Schematic representation of the coordination modes in the structure of $[\text{Cu}_{2.5}(\text{3-mpyf})(\text{N}_2)_{1.5}]_n$, a coordination polymer showing copper–dinitrogen coordination.



N,N'-bis(pyridine-3-ylmethyl)formamidinium or 3-Hmpyf (Figure 8.16). However, copper cations were also bridged by a diatomic donor, which was assigned as the dinitrogen derived from IR spectroscopy on isotopically labeled samples. The N–N stretching vibration was observed at $\sim 1575\text{ cm}^{-1}$, which indicates substantial activation of the N_2 donor and consistent with a one-electron reduced diazenyl (N_2^-) species. The formula of the coordination polymer was $[\text{Cu}_{2.5}(\text{3-mpyf})(\text{N}_2)_{1.5}]_n$, highlighting the incorporation of N_2 into the structure of this material in a ratio of three molecules of N_2 for each five copper atoms. Reduction of copper(II) to cuprous has precedent for reactions in alcohol solvents; however, the ease with which reduced dinitrogen donors are incorporated is surprising and unexpected as very strong reducing agents are typically required to synthesize metal diazenide complexes (e.g. alkali metals and potassium graphite). Arguably, deposition of copper metal is anticipated to be more facile than dinitrogen reduction.

Using a similar synthetic approach except with 4-(aminomethyl)-pyridine afforded the network solid containing *N,N'*-bis(pyridine-4-ylmethyl)-formamidinium (4-Hmpyf). In contrast to the 3-mpyf compound, the formamidinium is observed in the product with no evidence for protonation. The formula for this compound was found as $\{[\text{Cu}_3(\text{4-Hmpyf})(\text{N}_2)_3] \cdot (\text{CH}_3\text{OH})\}_n$. The structure showed a more complex arrangement of N_2 coordination modes to copper(I) centers, combining tricoordinate and tetracoordinate sites (Figure 8.17). As expected, there is a range of N–N bond distances throughout the structure of this compound from 1.152(6)–1.168(6) Å, which agrees with significant activation of the N_2 ligands.

8.3.1.3 Structural Relationships and Comparisons

Table 8.2 provides a summary of the N–N bond distances and the energies for the N–N stretching vibrational modes obtained for the reported copper–dinitrogen complexes.

As one can observe, with an exception of the coordination polymers $[\text{Cu}_{2.5}(\text{3-mpyf})(\text{N}_2)_{1.5}]_n$ and $\{[\text{Cu}_3(\text{4-Hmpyf})(\text{N}_2)_3] \cdot (\text{CH}_3\text{OH})\}_n$ reported by Hsu et al., the N–N distances of these compounds are close to the values for free dinitrogen (1.099 Å) [42]. This observation is consistent with a minimal N_2 activation

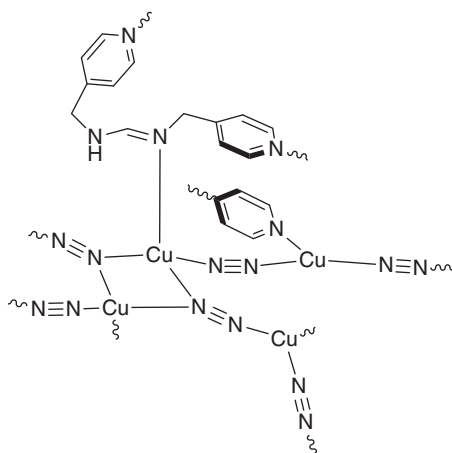


Figure 8.17 Schematic representation of the coordination around the copper centers in the structure of the coordination polymer $\{[\text{Cu}_3(4\text{-Hmpyf})(\text{N}_2)_3] \cdot (\text{CH}_3\text{OH})\}_n$.

Table 8.2 Structural data for the copper dinitrogen complexes: N—N bond distances and N—N stretching vibrational mode absorption energies.

| Compound | N—N distance (Å) | $\nu_{\text{N-N}}$ (cm^{-1}) | References |
|--|----------------------|---|------------|
| $\text{Cu}_2(\text{N}_2)$ | 1.095 ^{a)} | 2284 ^{b)} | [111] |
| $\text{Cu}_2(\text{N}_2)_2$ | 1.096 ^{a)} | 2272 ^{b)} , 2276 ^{b)} | [111] |
| $\text{CuCl}(\text{N}_2)$ | 1.100 ^{a)} | 2296.3 ^{b)} | [37] |
| $\text{CuBr}(\text{N}_2)$ | 1.100 ^{a)} | 2297.8 ^{b)} | [37] |
| $\text{CuF}(\text{N}_2)$ | 1.113 ^{a)} | n.r. | [110] |
| $\text{Cu}(\text{CO})(\text{N}_2)$ | 1.122 ^{a)} | 2066.4 ^{b)} | [112] |
| $\text{Cu}(\text{CO})(\text{N}_2)_2$ | 1.111 ^{a)} | 2088.0 ^{b)} | [112] |
| $[\text{Pr}_2\text{TpCu}]_2(\mu - \text{N}_2)$ | 1.110(6), 1.112(5) | 2130 ^{c)} | [115] |
| $\text{Cu}_3(\text{N}_2)\text{L}^{\text{Et/Me}}$ | 1.0854(1), 1.0956(1) | 1968, 1952 ^{c)} | [113] |
| $[\text{Cu}_{2.5}(3\text{-mpyf})(\text{N}_2)_{1.5}]_n$ | 1.168(4), 1.178(6) | 1574, 1576 ^{c)} | [116] |
| $\{[\text{Cu}_3(4\text{-Hmpyf})(\text{N}_2)_3] \cdot (\text{CH}_3\text{OH})\}_n$ | 1.152(6)–1.168(6) | 1603, 1607 ^{c)} | [116] |

a) Result from DFT calculations.

b) Obtained in a solid argon matrix between 11 and 25 K using $^{14}\text{N}_2$.

c) Result from Raman spectra.

n.r., not reported.

and agrees with the expected weak π -backbonding for copper. These values of bond distances translate to the high values for the N—N stretching mode found in the vibrational spectra of these compounds (2130–2298 cm^{-1}) compared to free nitrogen (2359 cm^{-1}) [1]. The only exception being the reported $\text{Cu}_3(\text{N}_2)\text{L}^{\text{Et/Me}}$ complex, which presented a low energy vibration at $\sim 1960 \text{ cm}^{-1}$ indicates a slightly activated N_2 fragment. Libration or other effects may lead to discrepancies between the crystallographic distance and the vibrational data. The enhanced activation relative to the dicopper compound reported by

Warren suggests cooperativity arising from the higher nuclearity. The effect of the number of metal ions on the extent of dinitrogen activation in multinuclear assemblies (e.g. tri- vs. dicopper species) is an area of active research for those focused on the chemistry of d- and f-block elements.

8.3.2 Silver and Gold

As observed for group 10, examples of dinitrogen metal compounds of the second- and third-row group 11 metals are unknown. In the case of silver and gold, no metal–dinitrogen compounds were found in which the dinitrogen ligand arises from free N_2 present in the reaction mixture.

Schmidt and collaborators have explored the interactions of small molecules to small cationic silver clusters ranging in nuclearity from 3 to 30 atoms (Ag_n^+). Using mass spectrometry in the fragmentation conditions to assess the strength of interactions, the binding energies of N_2 to these clusters were determined to be very small and consistent with a physisorption process [118, 119]. The authors also evaluated the use of mixtures of N_2 and O_2 because the latter is known to interact via chemisorption or, in other words, to bind strongly to these cationic clusters. From these experiments, binding O_2 to the clusters led to an enhancement of the binding of N_2 in the clusters, which is analogous to the CO results from the laser ablation studies on copper. This increase was attributed to charge transfer from the cluster to O_2 , which makes the cluster more electron deficient and, therefore, improving the acid–base interaction between the cluster and available N_2 molecules [118].

In the early 2000s, Kahani et al. published the first report of discrete coordination compounds of containing silver–dinitrogen bonds. The authors combined silver nitrate and ammonium peroxydisulfate in an ammonium hydroxide solution and in the presence of pyridine. Under these conditions, the silver centers and ammonia were oxidized to afford Ag(III) and N_2 , respectively, which formed the complex *trans*- $[Ag(py)_2(N_2)_2](OH)_3$ at high pH values. The counterions of this complex could also be exchanged to perchlorate upon exposure to excess $HClO_4$, resulting in the formation of *trans*- $[Ag(py)_2(N_2)_2](ClO_4)_3$. Both of these silver–dinitrogen compounds showed an absorption at 2157 cm^{-1} in their infrared spectra, which were assigned to the asymmetric stretching of the N–N bond, confirming the *trans* geometry. The minimal activation of the N_2 fragment is expected given the high oxidation state of the silver centers in these compounds [120].

In 2016, Wang et al. reported the synthesis of a diazenide-bridged silver(I) MOF. Here, the authors were exploring the use of a pincer ligand to stabilize and bind silver cations and the subsequent assembly of the silver species with polyoxometalate clusters to generate the framework [121]. Structure determination using single-crystal X-ray diffraction evidenced a ligand transformation as well as the incorporation of N_2^{2-} ligands. Relevant to this discussion, a N_2^{2-} ligand bridges two symmetrically related silver cations in an end-on manner, generating μ -1,2- N_2 linkages within the polymer. The N–N distance of $1.18(3)\text{ \AA}$ agrees with a relatively activated dinitrogen fragment, and it is in the range characteristic

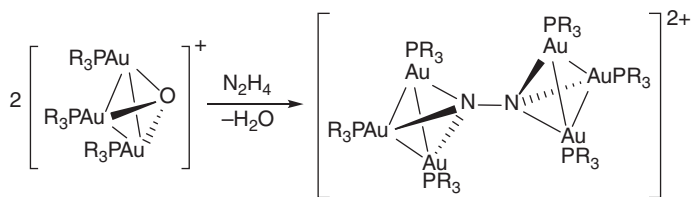


Figure 8.18 Synthesis of a dinitrogen-bridged hexagold cluster using different trisubstituted phosphines as supporting ligands ($\text{PR}_3 = \text{PPh}_2\text{Me}$, PPh_2Et , PPh_3 , $\text{P}(p\text{-MeC}_6\text{H}_5)_3$, $\text{P}(p\text{-MeOC}_6\text{H}_5)_3$, $\text{P}(p\text{-CF}_3\text{C}_6\text{H}_5)_3$, PPh_2Pr , and $\text{P}(o\text{-MeC}_6\text{H}_5)_3$).

of diazenyl or diazenido species [42]. Even though the authors report the vibrational spectrum for the resulting MOF, the assignment to N–N vibrational modes is unclear.

In the case of gold, the only example was reported by Shan et al. who studied multinuclear gold clusters stabilized by phosphines. They observed that the exposure of cationic trigold clusters of the type $[(\text{R}_3\text{PAu})_3(\mu\text{-O})]^+$ to excess anhydrous hydrazine led to the formation of hexagold clusters $[(\text{R}_3\text{PAu})_6(\text{N}_2)]^{2+}$ bridged by a N_2 fragment and release of oxide in the form of water (Figure 8.18) [122, 123]. The authors were able to obtain a solid-state structure of one of these clusters when phosphine used was isopropylidiphenylphosphine ($i\text{PrPh}_2\text{P}$). The observed N–N distance of 1.475(14) Å is one of the largest N–N distances for any metal–dinitrogen complex. This fact agrees with the synthetic protocol and the assignment of this N_2 fragment as hydrazido-hexagold species. Attempts to produce this cluster by direct activation of N_2 using analogous dicationic hexagold clusters did not result in any identifiable products. Despite the inability to bind and activate atmospheric dinitrogen, the authors demonstrated that these hexagold clusters can cleave the N–N bond to produce ammonia. The treatment of this family of N_2 -bridged gold clusters with reductants in the presence of proton sources produced mixtures of ammonia and hydrazine almost quantitatively. The product speciation in these cases were variable with respect of the phosphines used, indicating that both the basicity and the sterics of the different phosphorous-based ligands were responsible for the difference in reactivity.

8.4 Conclusion and Perspectives

As is apparent from the prior discussion, the chemistry of metal–dinitrogen compounds of groups 10 and 11 is dominated by complexes of nickel(0). This observation is consistent with nickel(0) being one of the least electronegative ions of the series and the particular broader community interest in small-molecule activation at late first-row transition metal centers. More broadly, the number of structurally characterized metal–dinitrogen complexes for groups 10 and 11 metals is miniscule in comparison to the earlier transition metals (groups 3–9); again, this trend reflects the ligand-field understanding of bonding within metal– N_2 fragments. With that said, however, recent reports highlight that the

coordination of dinitrogen to these metals is possible and critically depends on metal–ion oxidation state, choice of ancillary ligands, and steric effects. For example, lower valent metals, strongly donating ligands, and sterically encumbered coordination spheres – which discriminate between dinitrogen and larger potential ligands – are common themes. The majority of dinitrogen compounds show minimal activation of the bound dinitrogen, which has led to the primary use of these complexes as reactive starting materials for the activation of other substrates, such as CO₂, CO, and H₂. Addition of new group 10 and 11 compounds to the growing family of dinitrogen complexes will provide an important insight into metal–dinitrogen bonding interactions. More generally, such compounds will lead to a greater fundamental understanding of how changes in electronegativity impact, tune, and modulate metal–ligand bonding away from a classic ligand field theory approach as one approaches the p-block. For example, an unusual trend is that dinitrogen activation, as measured by vibrational spectroscopy, is enhanced in copper(I) complexes in the presence of π -acid donors; the ligand field expectation would be that competition for similar π -bonding orbitals would result in the opposite effect.

References

- 1 Holland, P.L. (2010). Metal–dioxygen and metal–dinitrogen complexes: where are the electrons? *Dalton Trans.* 39 (23): 5415–5425.
- 2 Ananikov, V.P. (2015). Nickel: the “spirited horse” of transition metal catalysis. *ACS Catal.* 5 (3): 1964–1971.
- 3 Khan, M.S., Haque, A., Al-Suti, M.K., and Raithby, P.R. (2015). Recent advances in the application of group-10 transition metal based catalysts in C–H activation and functionalization. *J. Organomet. Chem.* 793: 114–133.
- 4 Beeck, O. and Wheeler, A. (1939). Activated adsorption of nitrogen on iron at 23° and 100°C, and ammonia synthesis. *J. Chem. Phys.* 7 (8): 631–632.
- 5 Beeck, O., Smith, A.E., and Wheeler, A. (1940). Catalytic activity, crystal structure and adsorptive properties of evaporated metal films. *Proc. R. Soc. A* 177 (968): 62–90.
- 6 Mignolet, J.C.P. (1950). Studies in contact potentials. Part I.—The adsorption of some gases on evaporated nickel films. *Discuss. Faraday Soc.* 8: 105–114.
- 7 Beeck, O., Cole, W.A., and Wheeler, A. (1950). Determination of heats of adsorption using metal films. *Discuss. Faraday Soc.* 8: 314–321.
- 8 Trapnell, B.M.W. (1953). The activities of evaporated metal films in gas chemisorption. *Proc. R. Soc. A* 218 (1135): 566–577.
- 9 Wagener, S. (1957). Adsorption measurements at very low pressures. II. *J. Phys. Chem.* 61 (3): 267–271.
- 10 Selwood, P.W. (1958). The mechanism of chemisorption: nitrogen on nickel. *J. Am. Chem. Soc.* 80 (16): 4198–4201.
- 11 Kokes, R.J. and Emmett, P.H. (1960). Chemisorption of carbon monoxide, carbon dioxide and nitrogen on nickel catalysts. *J. Am. Chem. Soc.* 82 (5): 1037–1041.

- 12 Gundry, P.M., Haber, J., and Tompkins, F.C. (1962). Surface potential measurements on nickel and iron films during the chemisorption of ammonia, nitrogen, and hydrogen. *J. Catal.* 1 (4): 363–371.
- 13 van Hardeveld, R. and van Montfoort, A. (1966). The influence of crystallite size on the adsorption of molecular nitrogen on nickel, palladium and platinum. *Surf. Sci.* 4 (4): 396–430.
- 14 Horn, K., DiNardo, J., Eberhardt, W. et al. (1982). The adsorption of N₂: chemisorbed on Ni(110) and physisorbed on Pd(111). *Surf. Sci.* 118 (3): 465–495.
- 15 Brubaker, M.E. and Trenary, M. (1986). Adsorbate ordering processes and infrared spectroscopy: an FT-IRAS study of N₂ chemisorbed on the Ni(110) surface. *J. Chem. Phys.* 85 (10): 6100–6109.
- 16 Bertino, M., Steinhögl, W., Range, H. et al. (1996). The low-energy thermal excitation spectrum of nitrogen molecules adsorbed on Ni(110): implications for molecular adsorption sites. *Appl. Phys. A: Mater. Sci. Process.* 62 (2): 95–101.
- 17 Aleksandrov, H.A., Vayssilov, G.N., and Rösch, N. (2004). Theoretical investigation of the coordination of N₂ ligands to the cluster Ni₃. *J. Phys. Chem. A* 108 (29): 6127–6144.
- 18 Parks, E.K., Zhu, L., Ho, J., and Riley, S.J. (1994). The structure of small nickel clusters. I. Ni₃–Ni₁₅. *J. Chem. Phys.* 100 (10): 7206–7222.
- 19 Parks, E.K., Zhu, L., Ho, J., and Riley, S.J. (1995). The structure of small nickel clusters. II. Ni₁₆–Ni₂₈. *J. Chem. Phys.* 102 (19): 7377–7389.
- 20 Parks, E.K., Nieman, G.C., Kerns, K.P., and Riley, S.J. (1998). The thermodynamics of nitrogen adsorption on nickel clusters: Ni₁₉–Ni₇₁. *J. Chem. Phys.* 108 (9): 3731–3739.
- 21 Parks, E.K., Nieman, G.C., Kerns, K.P., and Riley, S.J. (1997). Reactions of Ni₃₈ with N₂, H₂, and CO: cluster structure and adsorbate binding sites. *J. Chem. Phys.* 107 (6): 1861–1871.
- 22 Dillinger, S., Mohrbach, J., and Niedner-Schatteburg, G. (2017). Probing cluster surface morphology by cryo spectroscopy of N₂ on cationic nickel clusters. *J. Chem. Phys.* 147 (18): 184305.
- 23 Mohrbach, J., Dillinger, S., and Niedner-Schatteburg, G. (2017). Probing cluster surface morphology by cryo kinetics of N₂ on cationic nickel clusters. *J. Chem. Phys.* 147 (18): 184304.
- 24 Burdett, J.K. and Turner, J.J. (1971). Binary transition metal nitrogen compounds; infrared evidence for Ni(N₂)_x. *J. Chem. Soc. D* 16: 885–886.
- 25 Burdett, J.K., Graham, M.A., and Turner, J.J. (1972). Binary compounds of dinitrogen with nickel, chromium, platinum, and copper: a vibrational investigation of the metal–dinitrogen linkage. *J. Chem. Soc., Dalton Trans.* (15): 1620–1625.
- 26 Moskovits, M. and Ozin, G.A. (1973). Matrix infrared spectroscopic evidence for “end-on” bonded dinitrogen in nickel monodinitrogen, NiN₂, and its relationship to dinitrogen chemisorbed on nickel. *J. Chem. Phys.* 58 (3): 1251–1252.
- 27 Huber, H., Kündig, E.P., Moskovits, M., and Ozin, G.A. (1973). Binary transition metal dinitrogen complexes. I. Matrix infrared and Raman spectra,

- structure and bonding of $\text{Ni}(\text{N}_2)_n$ and $\text{Pd}(\text{N}_2)_m$ ($n = 1-4$ and $m = 1-3$). *J. Am. Chem. Soc.* 95 (2): 332–344.
- 28 Barber, M. and Vickerman, J.C. (1974). An investigation of the $\text{Ni}/\text{N}_2\text{O}$ system by secondary ion mass spectrometry. *Chem. Phys. Lett.* 26 (2): 277–280.
- 29 Dubs, L. and R. and McKoy, V. (1987). Studies of NiN_2 as a model for photoemission from N_2 adsorbed on nickel. *Chem. Phys. Lett.* 142 (3–4): 237–240.
- 30 Ohno, M. and von Niessen, W. (1991). Many-body calculation of the valence photoemission spectrum of NiN_2 . *Phys. Rev. B* 44 (4): 1896–1903.
- 31 Manceron, L., Alikhani, M.E., and Joly, H.A. (1998). Infrared matrix isolation and DFT study of NiN_2 . *Chem. Phys.* 228 (1–3): 73–80.
- 32 Hübner, O., Manceron, L., and Himmel, H.-J. (2014). On the electronic structure and photochemistry of coordinatively unsaturated complexes: the case of nickel bis-dinitrogen, $\text{Ni}(\text{N}_2)_2$. *Chem. Eur. J.* 20 (51): 17025–17038.
- 33 Himmel, H.-J. and Manceron, L. (2005). $\text{Ni}(\text{N}_2)_4$ revisited: an analysis of the $\text{Ni}-\text{N}_2$ bonding properties of this benchmark system on the basis of UV/Vis, IR and Raman spectroscopy. *Dalton Trans.* 0 (15): 2615.
- 34 Rest, A.J. (1972). IR evidence for tricarbonyl(dinitrogen) nickel, $\text{Ni}(\text{CO})_3(\text{N}_2)$, in a nitrogen matrix at 20 K. *J. Organomet. Chem.* 40 (2): C76–C78.
- 35 Kündig, E.P., Moskovits, M., and Ozin, G.A. (1973). Binary mixed dinitrogen–carbonyl complexes of nickel(0), $\text{Ni}(\text{N}_2)_m(\text{CO})_{4-m}$ (where $m = 1-3$). *Can. J. Chem.* 51 (16): 2737–2746.
- 36 Turner, J.J., Simpson, M.B., Poliakoff, M., and Maier, W.B. III (1983). Synthesis and decay kinetics of $\text{Ni}(\text{CO})_3\text{N}_2$ in liquid krypton: approximate determination of the $\text{Ni}-\text{N}_2$ bond dissociation energy. *J. Am. Chem. Soc.* 105 (12): 3898–3904.
- 37 Chen, M., Zhou, M., Zhang, L., and Qin, Q. (2000). Matrix-isolation FTIR spectroscopic and DFT studies of the XMNN ($\text{X}=\text{Cl}, \text{Br}$, $\text{M}=\text{Cu}, \text{Ni}$) molecules. *J. Phys. Chem. A* 104 (38): 8627–8631.
- 38 Bridgeman, A.J., Wilkin, O.M., and Young, N.A. (2000). Dinitrogen bonding modes to molecular nickel(II) halides: a matrix isolation IR and DFT study. *Inorg. Chem. Commun.* 3 (12): 681–684.
- 39 Jonas, K. (1973). π -bonded nitrogen in a crystalline nickel–lithium complex. *Angew. Chem. Int. Ed. Engl.* 12 (12): 997–998.
- 40 Krüger, C. and Tsay, Y.-H. (1973). Molecular structure of a π -dinitrogen–nickel–lithium complex. *Angew. Chem. Int. Ed. Engl.* 12 (12): 998–999.
- 41 Jonas, K., Brauer, D.J., Krüger, C. et al. (1976). “Side-on” dinitrogen–transition metal complexes. The molecular structure of $\{\text{C}_6\text{H}_5[\text{Na}\cdot\text{O}(\text{C}_2\text{H}_5)_2]_2[(\text{C}_6\text{H}_5)_2\text{Ni}]_2\text{N}_2\text{NaLi}_6(\text{OC}_2\text{H}_5)_4\cdot\text{O}(\text{C}_2\text{H}_5)_2\}_2$. *J. Am. Chem. Soc.* 98 (1): 74–81.
- 42 Peigné, B. and Aullón, G. (2015). Structural analysis of the coordination of dinitrogen to transition metal complexes. *Acta Crystallogr., Sect. B: Struct. Sci. Cryst. Eng. Mater.* 71 (3): 369–386.

- 43 Tolman, C.A., Seidel, W.C., and Gosser, L.W. (1974). Formation of three-coordinate nickel(0) complexes by phosphorus ligand dissociation from NiL_4 . *J. Am. Chem. Soc.* 96 (1): 53–60.
- 44 Tolman, C.A., Gerlach, D.H., Jesson, J.P., and Schunn, R.A. (1974). Reaction of nitrogen with triethylphosphine complexes of zero-valent Ni, Pd, and Pt: evidence for a nickel dinitrogen complex. *J. Organomet. Chem.* 65 (1): C23–C26.
- 45 Jolly, P.W. and Jonas, K. (1968). Fixation of molecular nitrogen on nickel(0). *Angew. Chem. Int. Ed. Engl.* 7 (9): 731–732.
- 46 Jolly, P.W., Jonas, K., Krüger, C., and Tsay, Y.-H. (1971). The preparation, reactions and structure of bis[bis(tricyclohexylphosphine)nickel] dinitrogen, $\{[(\text{C}_6\text{H}_{11})_3\text{P}]_2\text{Ni}\}_2\text{N}_2$. *J. Organomet. Chem.* 33 (1): 109–122.
- 47 Aresta, M., Nobile, C.F., and Sacco, A. (1975). Tertiary phosphine complexes of nickel(0) and nickel(I). New dinitrogen complexes of nickel(0). *Inorg. Chim. Acta* 12 (1): 167–178.
- 48 Osakada, K., Hayashi, H., Maeda, M. et al. (1986). Preparation and properties of new thiolato- and mercapto–transition metal complexes, $\text{MR}(\text{SR}')(\text{PR}''_3)_2$ ($\text{M} = \text{Ni}, \text{Pd}$; $\text{R} = \text{H}, \text{Ar}$; $\text{R}' = \text{H}, \text{Ar}$). Evolution of $\text{R}-\text{R}'$ from the complexes through cleavage of the $\text{S}-\text{R}'$ bond. *Chem. Lett.* 15 (4): 597–600.
- 49 Aresta, M., Quaranta, E., and Tommasi, I. (1988). Reduction of co-ordinated carbon dioxide to carbon monoxide via protonation by thiols and other Brønsted acids promoted by Ni-systems: a contribution to the understanding of the mode of action of the enzyme carbon monoxide dehydrogenase. *J. Chem. Soc., Chem. Commun.* (7): 450–452.
- 50 Beck, R., Shoshani, M., Krasinkiewicz, J. et al. (2013). Synthesis and chemistry of bis(triisopropylphosphine) nickel(I) and nickel(0) precursors. *Dalton Trans.* 42 (5): 1461–1475.
- 51 Tolman, C.A. (1977). Steric effects of phosphorus ligands in organometallic chemistry and homogeneous catalysis. *Chem. Rev.* 77 (3): 313–348.
- 52 Waterman, R. and Hillhouse, G.L. (2005). Synthesis and structure of a terminal dinitrogen complex of nickel. *Can. J. Chem.* 83 (4): 328–331.
- 53 Bach, I., Goddard, R., Kopsike, C. et al. (1999). Synthesis, structure, and reactivity of $(^t\text{Bu}_2\text{PC}_2\text{H}_4\text{P}^t\text{Bu}_2)\text{Ni}(\text{CH}_3)_2$ and $\{(^t\text{Bu}_2\text{PC}_2\text{H}_4\text{P}^t\text{Bu}_2)\text{Ni}\}_2(\mu\text{-H})_2$. *Organometallics* 18 (1): 10–20.
- 54 Kim, Y.-E., Kim, J., and Lee, Y. (2014). Formation of a nickel carbon dioxide adduct and its transformation mediated by a Lewis acid. *Chem. Commun.* 50 (78): 11458–11461.
- 55 Kim, Y.-E., Oh, S., Kim, S. et al. (2015). Phosphinite-Ni(0) mediated formation of a phosphide-Ni(II)-OCOOME species via uncommon metal–ligand cooperation. *J. Am. Chem. Soc.* 137 (13): 4280–4283.
- 56 Oh, S., Kim, S., Lee, D. et al. (2016). Alkoxide migration at a nickel(II) center induced by a π -acidic ligand: migratory insertion versus metal–ligand cooperation. *Inorg. Chem.* 55 (24): 12863–12871.
- 57 Mankad, N.P., Rivard, E., Harkins, S.B., and Peters, J.C. (2005). Structural snapshots of a flexible Cu_2P_2 core that accommodates the oxidation states Cu^ICu^I , $\text{Cu}^{1.5}\text{Cu}^{1.5}$, and $\text{Cu}^{II}\text{Cu}^{II}$. *J. Am. Chem. Soc.* 127 (46): 16032–16033.

- 58 Suh, H.-W., Schmeier, T.J., Hazari, N. et al. (2012). Experimental and computational studies of the reaction of carbon dioxide with pincer-supported nickel and palladium hydrides. *Organometallics* 31 (23): 8225–8236.
- 59 Charboneau, D.J., Balcells, D., Hazari, N. et al. (2016). Dinitrogen-facilitated reversible formation of a Si–H bond in a pincer-supported Ni complex. *Organometallics* 35 (18): 3154–3162.
- 60 Harman, W.H., Lin, T.-P., and Peters, J.C. (2014). A d^{10} Ni–(H₂) adduct as an Intermediate in H–H oxidative addition across a Ni–B bond. *Angew. Chem. Int. Ed.* 53 (4): 1081–1086.
- 61 Harman, W.H. and Peters, J.C. (2012). Reversible H₂ addition across a nickel-borane unit as a promising strategy for catalysis. *J. Am. Chem. Soc.* 134 (11): 5080–5082.
- 62 Connelly, S.J., Zimmerman, A.C., Kaminsky, W., and Heinekey, D.M. (2012). Synthesis, structure, and reactivity of a nickel dihydrogen complex. *Chem. Eur. J.* 18 (50): 15932–15934.
- 63 Zhu, D., Thapa, I., Korobkov, I. et al. (2011). Redox-active ligands and organic radical chemistry. *Inorg. Chem.* 50 (20): 9879–9887.
- 64 Lyaskovskyy, V. and de Bruin, B. (2012). Redox non-innocent ligands: versatile new tools to control catalytic reactions. *ACS Catal.* 2 (2): 270–279.
- 65 Cowie, B.E. and Emslie, D.J.H. (2015). Nickel and palladium complexes of ferrocene-backbone bisphosphine-borane and trisphosphine ligands. *Organometallics* 34 (16): 4093–4101.
- 66 Mankad, N.P., Whited, M.T., and Peters, J.C. (2007). Terminal Fe^I–N₂ and Fe^{II}···H–C interactions supported by tris(phosphino)silyl ligands. *Angew. Chem. Int. Ed.* 46 (30): 5768–5771.
- 67 Lee, Y., Mankad, N.P., and Peters, J.C. (2010). Triggering N₂ uptake via redox-induced expulsion of coordinated NH₃ and N₂ silylation at trigonal bipyramidal iron. *Nat. Chem.* 2 (7): 558–565.
- 68 Moret, M.-E. and Peters, J.C. (2011). Terminal iron dinitrogen and iron imide complexes supported by a tris(phosphino)borane ligand. *Angew. Chem. Int. Ed.* 50 (9): 2063–2067.
- 69 Moret, M.-E. and Peters, J.C. (2011). N₂ Functionalization at iron metallaboratranes. *J. Am. Chem. Soc.* 133 (45): 18118–18121.
- 70 Anderson, J.S., Moret, M.-E., and Peters, J.C. (2013). Conversion of Fe–NH₂ to Fe–N₂ with release of NH₃. *J. Am. Chem. Soc.* 135 (2): 534–537.
- 71 Anderson, J.S., Rittle, J., and Peters, J.C. (2013). Catalytic conversion of nitrogen to ammonia by an iron model complex. *Nature* 501 (7465): 84–87.
- 72 Creutz, S.E. and Peters, J.C. (2014). Catalytic reduction of N₂ to NH₃ by an Fe–N₂ complex featuring a C-atom anchor. *J. Am. Chem. Soc.* 136 (3): 1105–1115.
- 73 Anderson, J.S., Cutsail, G.E. III, Rittle, J. et al. (2015). Characterization of an Fe≡N–NH₂ intermediate relevant to catalytic N₂ reduction to NH₃. *J. Am. Chem. Soc.* 137 (24): 7803–7809.
- 74 Del Castillo, T.J., Thompson, N.B., and Peters, J.C. (2016). A synthetic single-site Fe nitrogenase: high turnover, freeze-quench ⁵⁷Fe Mössbauer data, and a hydride resting state. *J. Am. Chem. Soc.* 138 (16): 5341–5350.

- 75 Tsay, C. and Peters, J.C. (2012). Thermally stable N_2 and H_2 adducts of cationic nickel(II). *Chem. Sci.* 3 (4): 1313–1318.
- 76 Sircoglou, M., Bontemps, S., Bouhadir, G. et al. (2008). Group 10 and 11 metal boratranes (Ni, Pd, Pt, CuCl, AgCl, AuCl, and Au^+) derived from a triphosphine-borane. *J. Am. Chem. Soc.* 130 (49): 16729–16738.
- 77 Cammarota, R.C. and Lu, C.C. (2015). Tuning nickel with Lewis acidic group 13 metalloligands for catalytic olefin hydrogenation. *J. Am. Chem. Soc.* 137 (39): 12486–12489.
- 78 Rudd, P.A., Liu, S., Gagliardi, L. et al. (2011). Metal–alane adducts with zero-valent nickel, cobalt, and iron. *J. Am. Chem. Soc.* 133 (51): 20724–20727.
- 79 Pfirrmann, S., Limberg, C., Herwig, C. et al. (2009). A dinuclear nickel(I) dinitrogen complex and its reduction in single-electron steps. *Angew. Chem. Int. Ed.* 48 (18): 3357–3361.
- 80 Horn, B., Pfirrmann, S., Limberg, C. et al. (2011). N_2 activation in Ni^I –NN– Ni^I units: the influence of alkali metal cations and CO reactivity. *Z. Anorg. Allg. Chem.* 637 (9): 1169–1174.
- 81 Figg, T.M., Holland, P.L., and Cundari, T.R. (2012). Cooperativity between low-valent iron and potassium promoters in dinitrogen fixation. *Inorg. Chem.* 51 (14): 7546–7550.
- 82 Horn, B., Limberg, C., Herwig, C., and Mebs, S. (2011). The conversion of nickel-bound CO into an acetyl thioester: organometallic chemistry relevant to the acetyl coenzyme A synthase active site. *Angew. Chem. Int. Ed.* 50 (52): 12621–12625.
- 83 Holze, P., Horn, B., Limberg, C. et al. (2014). The Activation of sulfur hexafluoride at highly reduced low-coordinate nickel dinitrogen complexes. *Angew. Chem. Int. Ed.* 53 (10): 2750–2753.
- 84 Chavan, S., Bonino, F., Vitillo, J.G. et al. (2009). Response of CPO-27-Ni towards CO, N_2 and C_2H_4 . *Phys. Chem. Chem. Phys.* 11 (42): 9811–9822.
- 85 Dietzel, P.D.C., Panella, B., Hirscher, M. et al. (2006). Hydrogen adsorption in a nickel based coordination polymer with open metal sites in the cylindrical cavities of the desolvated framework. *Chem. Commun.* (9): 959–961.
- 86 Vitillo, J.G., Regli, L., Chavan, S. et al. (2008). Role of exposed metal sites in hydrogen storage in MOFs. *J. Am. Chem. Soc.* 130 (26): 8386–8396.
- 87 Wu, H., Zhou, W., and Yildirim, T. (2009). High-capacity methane storage in metal-organic frameworks M_2 (dhtp): the important role of open metal sites. *J. Am. Chem. Soc.* 131 (13): 4995–5000.
- 88 Dietzel, P.D.C., Johnsen, R.E., Fjellvåg, H. et al. (2008). Adsorption properties and structure of CO_2 adsorbed on open coordination sites of metal-organic framework Ni_2 (dhtp) from gas adsorption, IR spectroscopy and X-ray diffraction. *Chem. Commun.* (41): 5125–5127.
- 89 McKinlay, A.C., Xiao, B., Wragg, D.S. et al. (2008). Exceptional behavior over the whole adsorption-storage-delivery cycle for NO in porous metal organic frameworks. *J. Am. Chem. Soc.* 130 (31): 10440–10444.

- 90 Bonino, F., Chavan, S., Vitillo, J.G. et al. (2008). Local structure of CPO-27-Ni metallorganic framework upon dehydration and coordination of NO. *Chem. Mater.* 20 (15): 4957–4968.
- 91 Kündig, E.P., Moskovits, M., and Ozin, G.A. (1973). Binary transition metal dinitrogen complexes. Part II. Matrix infrared and Raman spectra, structure, and bonding of $\text{Pt}(\text{N}_2)_n$ (where $n = 1-3$). *Can. J. Chem.* 51 (16): 2710–2721.
- 92 Klotzbücher, W. and Ozin, G.A. (1975). Binary transition metal dinitrogen complexes. III. Metal–nitrogen stretching modes of $\text{Ni}(\text{N}_2)_n$, $\text{Pd}(\text{N}_2)_m$, and $\text{Pt}(\text{N}_2)_m$ (where $n = 1-4$ and $m = 1-3$). *J. Am. Chem. Soc.* 97 (10): 2672–2675.
- 93 Schrittenlacher, W., Schroeder, W., Rotermund, H.H. et al. (1986). The optical spectra of matrix-isolated palladium–nitrogen complexes: an investigation by absorption, emission, and photoelectron spectroscopy. *J. Chem. Phys.* 85 (3): 1348–1354.
- 94 Ozin, G.A. and Garcia-Prieto, J. (1988). Optical spectra of coexisting $^1\text{S}_0$ and $^3\text{D}_3$ palladium atoms and $^1\Sigma^+$ and $^3\Sigma^+$ $\text{Pd}(\text{N}_2)$ binary palladium–dinitrogen molecules isolated in argon matrices. A study by UV–visible absorption, broad-band and laser-induced fluorescence, and infrared and Raman spectroscopies. *J. Phys. Chem.* 92 (2): 325–337.
- 95 Citra, A., Wang, X., Bare, W.D., and Andrews, L. (2001). Reactions of laser-ablated platinum with nitrogen: matrix infrared spectra of platinum nitride, complexes, and anions. *J. Phys. Chem. A* 105 (33): 7799–7811.
- 96 Souvi, S.M., Tremblay, B., Perchard, J.P., and Alikhani, M.E. (2009). Pd_2N_2 , a proteiform molecule: matrix isolation spectroscopy and density functional theory calculations. *J. Chem. Phys.* 130 (7): 74304.
- 97 Ozin, G.A. and Klotzbücher, W.E. (1975). Binary mixed dioxygen dinitrogen complexes of nickel, palladium, and platinum, $(\text{O}_2)\text{M}(\text{N}_2)_n$ (where M = nickel, palladium, or platinum; $n = 1$ or 2). *J. Am. Chem. Soc.* 97 (14): 3965–3974.
- 98 Du, Y., Zhang, N., Cui, M. et al. (2012). Investigation on the hydrolysis of the anticancer drug cisplatin by Fourier transform ion cyclotron resonance mass spectrometry. *Rapid Commun. Mass Spectrom.* 26 (23): 2832–2836.
- 99 Xie, F., Colin, P., and Van Bocxlaer, J. (2017). Electrospray ionization mass spectrometry for the hydrolysis complexes of cisplatin: implications for the hydrolysis process of platinum complexes. *J. Mass Spectrom.* 52 (7): 434–441.
- 100 Kuroda, Y., Konno, S., Morimoto, K., and Yoshikawa, Y. (1993). Strong adsorption of dinitrogen on copper-ion-exchanged mordenite at room temperature. *J. Chem. Soc., Chem. Commun.* 1: 18–20.
- 101 Kuroda, Y., Yoshikawa, Y., Konno, S. et al. (1995). Specific feature of copper ion-exchanged mordenite for dinitrogen adsorption at room temperature. *J. Phys. Chem.* 99 (26): 10621–10628.
- 102 Spoto, G., Bordiga, S., Ricchiardi, G. et al. (1995). Formation of $\text{Cu}^{\text{I}}-\text{N}_2$ adducts at 298 and 77 K in $\text{Cu}^{\text{I}}\text{-ZSM-5}$: an FTIR investigation. *J. Chem. Soc., Faraday Trans.* 91 (18): 3285–3290.

- 103 Kuroda, Y., Yoshikawa, Y., Emura, S. et al. (1999). Characterization of specific N_2 -adsorption site existing on CuZSM-5 type zeolite: effect of ion-exchange level on adsorption properties. *J. Phys. Chem. B* 103 (12): 2155–2164.
- 104 Grünert, W., Hayes, N.W., Joyner, R.W. et al. (1994). Structure, chemistry, and activity of Cu-ZSM-5 catalysts for the selective reduction of NO_x in the presence of oxygen. *J. Phys. Chem.* 98 (42): 10832–10846.
- 105 Woertink, J.S., Smeets, P.J., Groothaert, M.H. et al. (2009). A $[Cu_2O]^{2+}$ core in Cu-ZSM-5, the active site in the oxidation of methane to methanol. *Proc. Natl. Acad. Sci. U.S.A.* 106 (45): 18908–18913.
- 106 Smeets, P.J., Hadt, R.G., Woertink, J.S. et al. (2010). Oxygen precursor to the reactive intermediate in methanol synthesis by Cu-ZSM-5. *J. Am. Chem. Soc.* 132 (42): 14736–14738.
- 107 Tsai, M.-L., Hadt, R.G., Vanelderen, P. et al. (2014). $[Cu_2O]^{2+}$ active site formation in Cu-ZSM-5: geometric and electronic structure requirements for N_2O activation. *J. Am. Chem. Soc.* 136 (9): 3522–3529.
- 108 Zeppenfeld, P., Goerge, J., Diercks, V. et al. (1997). Orientational ordering on a corrugated substrate: novel pinwheel structure for N_2 adsorbed on Cu(110). *Phys. Rev. Lett.* 78 (8): 1504–1507.
- 109 Ohshimo, K., Mizuuchi, I., Akimoto, K. et al. (2017). Mass spectrometric study of N_2 -adsorption on copper cluster cations formed by modulated pulsed power magnetron sputtering in aggregation cell. *Chem. Phys. Lett.* 682: 60–63.
- 110 Francis, S.G., Matthews, S.L., Poleshchuk, O.K. et al. (2006). N_2 –Cu–F: a complex of dinitrogen and cuprous fluoride characterized by rotational spectroscopy. *Angew. Chem. Int. Ed.* 45 (38): 6341–6343.
- 111 Elustondo, F., Mascetti, J., and Pápai, I. (2000). Identification of $Cu_2(N_2)$ and $Cu_2(N_2)_2$ complexes: matrix isolation and density functional studies. *J. Phys. Chem. A* 104 (16): 3572–3578.
- 112 Lu, Z.-H. and Xu, Q. (2010). CO-promoted N_2 adsorption on copper atoms. *Phys. Chem. Chem. Phys.* 12 (26): 7077–7082.
- 113 Murray, L.J., Weare, W.W., Shearer, J. et al. (2014). Isolation of a (dinitrogen)tricopper(I) complex. *J. Am. Chem. Soc.* 136 (39): 13502–13505.
- 114 Di Francesco, G.N., Gaillard, A., Ghiviriga, I. et al. (2014). Modeling biological copper clusters: synthesis of a tricopper complex, and its chloride- and sulfide-bridged congeners. *Inorg. Chem.* 53 (9): 4647–4654.
- 115 Zhang, S., Fallah, H., Gardner, E.J. et al. (2016). A dinitrogen dicopper(I) complex via a mixed-valence dicopper hydride. *Angew. Chem. Int. Ed.* 55 (34): 9927–9931.
- 116 Hsu, W., Thapa, K.B., Yang, X.-K. et al. (2016). Dinitrogen-supported coordination polymers. *CrystEngComm* 18 (3): 390–393.
- 117 Hsu, W., Chen, K.-T., Li, Y.-S. et al. (2014). Crystal-to-crystal transformations and photoluminescence changes in the Cu(I) coordination networks based on a formamidinate ligand. *CrystEngComm* 16 (46): 10640–10648.
- 118 Schmidt, M., Masson, A., and Bréchnignac, C. (2005). Enhancement of nitrogen physisorption in coadsorption with oxygen on free, positively charged silver clusters. *J. Chem. Phys.* 122 (13): 134712.

- 119 Wu, Y.-N., Schmidt, M., Leygnier, J. et al. (2012). Adsorption of small molecules on silver clusters. *J. Chem. Phys.* 136 (2): 024314.
- 120 Kahani, A., Abedini, M., and Farnia, M. (2001). Synthesis of new pyridine silver(III) complexes. *J. Coord. Chem.* 53 (1): 1–6.
- 121 Wang, X., Rong, X., Lin, H. et al. (2016). A novel Wells–Dawson polyoxometalate-based metal–organic framework constructed from the uncommon in-situ transformed bi(triazole) ligand and azo anion. *Inorg. Chem. Commun.* 63: 30–34.
- 122 Kolb, A., Bissinger, P., and Schmidbaur, H. (1993). Some tris[(triorganophosphine)gold(I)]-oxonium and -organoimonium tetrafluoroborates with bulky substituents. *Z. Anorg. Allg. Chem.* 619 (9): 1580–1588.
- 123 Shan, H., Yang, Y., James, A.J., and Sharp, P.R. (1997). Dinitrogen bridged gold clusters. *Science* 275 (5305): 1460–1462.